Article:
Hodgson, DM orcid.org/0000-0003-3711-635X, Brooks, HL, Ortiz-Karpf, A et al. (3 more authors) (2018) Entrainment and abrasion of megaclasts during submarine landsliding and their impact on flow behaviour. Geological Society Special Publications, 477. ISSN 0305-8719

https://doi.org/10.1144/SP477.26

The entrainment and abrasion of megaclasts during submarine landsliding and their impact on flow behaviour

Hodgson, D.M.[1], Brooks, H.L.[1], Ortiz-Karpf, A.[1,3], Spychala, Y.[1,4], Lee, D.R.[1], Jackson C.A-L.[2]*

[1]Stratigraphy Group, School of Earth and Environment, University of Leeds, Leeds, LS2 9JT

[2]Basins Research Group (BRG), Department of Earth Science & Engineering, Imperial College, Prince Consort Road, London, SW7 2BP, UK

[3]Present address: Ecopetrol, Cra. 13 #36-24, Bogotá, Colombia

[4]Present address: University of Utrecht, Heidelberglaan 2, 3584 CS Utrecht, The Netherlands

*Correspondence (d.hodgson@leeds.ac.uk)

Abstract: Many mass transport complexes (MTCs) contain up to kilometre-scale (mega)clasts encased in a debritic matrix. Although many megaclasts are sourced from headwall areas, the irregular basal shear surfaces of many MTCs indicates megaclast entrainment during the passage of flows into the deeper basin is also common. However, the mechanisms responsible for entrainment of large blocks of substrate, and their influence on the longitudinal behaviour of their associated flows, have not been widely considered. We here present examples of megaclasts from exhumed MTCs (Neuquén Basin, Argentina, and Karoo Basin, South Africa) and MTCs imaged in 3D seismic reflection data (Magdalena Fan, offshore Colombia and Santos Basin, offshore Brazil) to investigate these process-product interactions. We show that highly sheared basal surfaces are well-developed in distal locations, sometimes extending beyond their associated deposit. This points to deformation and weakening of the substrate ahead of the flow, suggesting preconditioning of the substrate by distributed shear ahead of, and to the side of, a mass flow could result in entrainment of large fragments. An improved understanding of the interactions between flow evolution, seabed topography, and entrainment and abrasion of megaclasts will help to refine estimates of runout distances, and therefore geohazard potential, of submarine landslides.

A major volumetric component of some submarine mass transport complexes (MTCs) are megaclasts; these are blocks of relatively undeformed strata that can be carried by sediment gravity currents due to the high cohesive strength of the muddy matrix (e.g. Marr *et al.* 2001; Lee *et al*. 2004; Kvalstad *et al.* 2005; Moscardelli *et al.* 2006; Bull *et al*. 2009; Dunlap *et al*. 2010). Megaclasts span a wide range of sizes, ranging from greater than boulder (4.1 m diameter; Blair & McPherson 1999), to kms in length, and 100's m in height, and are thus synonymous with 'blocks', 'rafts', and 'olistoliths' (e.g. Lucente & Pini 2003; Bull *et al.* 2009; Festa *et al*. 2016). Megaclasts are identified and characterized in outcrops (e.g. Lucenete & Pini 2003; Dykstra *et al.* 2011; Alves 2015; Sobiesiak *et al.* 2016; Brooks *et al.* 2017) and high-resolution seismic reflection data (e.g. McGilvery *et al.* 2004; Jackson 2011; Watt *et al.* 2012; Olafiranye *et al.* 2013). Subsurface studies have been particularly insightful, allowing the distribution of megaclasts to be constrained (e.g. Moscardelli *et al*. 2006; Jackson 2011; Ortiz-Karpf *et al.* 2017), and highlighting the influence they may have on subsequent flow processes and stratal architecture (e.g. Jackson & Johnson 2009; Ortiz-Karpf *et al*. 2015; 2017; Kneller *et al.* 2016). Erosion at the base of megaclasts may also explain the development of linear scours (Moscardelli *et al*. 2006) identified on the basal shear surface of seismically imaged MTCs; such features may be used as kinematic indicators that define the bulk flow direction of the parent flow (e.g. Posamentier & Kolla 2003; McGilvery *et al.* 2004). Seismic reflection data also permit detailed study of the internal structure of megaclasts, indicating deformation can occur before, during, and after transport in the parent flow, revealing much about flow rheology and related stresses (e.g., Lucente & Pini 2003; Bull *et al.* 2009; Jackson 2011). Furthermore, these data allow assessment of the role of megaclasts in hydrocarbon exploration and development in deep-water systems (e.g. Gamboa & Alves 2015; Alves 2015). It is therefore important to understand the origin and distribution of megaclasts, and their influence on flow rheology and evolution.

Megaclasts are either sourced from the protolith in a headwall area, or entrained from the basal or lateral substrate during emplacements of the mass flow (Piper *et al.* 1997; Sobiesiak *et al*. 2016). Headwall-sourced megaclasts may travel only short distances downdip (e.g. Alves 2015), or may be transported several tens to hundreds of kilometres by sliding over the basal shear surface (e.g. Hampton *et al.* 1996; Mohrig *et al.* 1999). The size of megaclasts sourced

from the headwall region is controlled by a number of factors, including excess pore pressure, strain softening, the mechanism of sliding (Kvalstad *et al.* 2005), and pressure build-up at their bases (Alves 2015). After initial slope failure, headwall-sourced megaclasts may move downslope and become fragmented by a combination of sliding (Hampton *et al.* 1996; Masson *et al.* 1997; Mohrig *et al.* 1999), rotation, and rolling (Gee *et al.* 2006; Lourenço *et al.* 2006) processes. The basal shear surface of an MTC can be highly erosional (e.g. Moscardelli *et al.* 2006; Alves and Cartwright 2009; Sawyer *et al.* 2009; Dakin *et al.* 2013; Ortiz Karpf *et al.* 2015; Fig. 1), comprising ramps and flats (e.g. Lucente & Pini 2003), scours and grooves. The basal shear surface may be represented by a zone of distributed strain rather than a discrete surface (e.g. Alves & Lourenço, 2010).

Megaclasts may also be entrained from the lateral margins of basal shear surfaces; in this case, shear is accommodated either by strike-slip faults striking sub-parallel to the parent flow direction (Martinsen 1994; Alves & Cartwright 2009; Alves 2015), or by normal faults that face inwards towards the flow/deposit (Bull *et al.* 2009). Irrespective of whether material is entrained from the basal or lateral substrate, it is clear these processes cause submarine landslides to ingest large volumes of substrate during their emplacement (e.g. Dykstra *et al.* 2011; Dakin *et al.* 2013), such that their final volume is far greater than that of material that initially failed from the headwall region (e.g. Gee *et al.* 2006; Alves & Cartwright, 2009; Butler & McCaffrey 2010; Fig. 1). However, the precise mechanisms for entraining megaclasts, and their influence on the subsequent rheology of the associated flow evolution, is poorly understood.

Here, we investigate the origin of megaclasts and their impact on flow rheology contained within erosionally based, stratigraphically chaotic units, using examples of exhumed MTCs exposed in the Neuquén Basin, Argentina and the Karoo Basin, South Africa, and imaged in 3D seismic reflection data from offshore Colombia and offshore Brazil (Fig. 2). Outcrop examples allow us to study the detailed composition and structure of megaclasts, whereas seismically imaged examples allow us to place megaclasts in their correct spatial position with respect to erosional features along the basal shear surface and in their overall context within the larger submarine slope system. Our specific objectives are: i) to describe the megaclasts

92 and infer the rheology of their host flow, ii) to discuss the mechanisms for entrainment of
93 substrate during the passage of the flow, and iii) to consider how megaclast abrasion during
94 transport can influence flow processes.

95

96 **Subsurface Examples**

97

98 *General seismic expression*

99 MTCs offshore Colombia and Brazil (Fig. 2) display many of the criteria typically used to
100 identify MTCs in seismic reflection data (cf. Posamentier and Kolla, 2003; Lee *et al.* 2004;
101 McGilvery *et al.* 2004; Moscardelli *et al.* 2006; Bull *et al.* 2009). First, the majority of these
102 deposits (>95%) are dominated by chaotic, low-amplitude seismic reflections that we
103 interpret as deposits of mud-rich debris flows (debrites). The top surfaces are rugose, which
104 is related to a combination of the high yield strength of the debrite-dominated portion of
105 these deposits, and the structurally coherent megaclasts protruding above their upper
106 surfaces (Fig. 3). Second, the MTCs are underlain by a sharp, erosional surface, which we
107 interpret as the "basal shear surface" (i.e. the surface above which the MTC was translated
108 and deposited; e.g. Posamentier and Kolla 2003; Lee *et al.* 2004; McGilvery *et al.* 2004;
109 Moscardelli *et al.* 2006; Bull *et al.* 2009; Alves and Lourenço 2010). A series of elongate
110 lineaments, which are best-expressed in map view, occur on the basal shear surface. These
111 are 'V'-shaped in cross section and are interpreted as grooves or striations (*sensu* Bull *et al.*
112 2009) created by and during passage of the parent flow. Irrespective of the process origin of
113 the grooves, we can use these features as kinematic indicators to infer the local or regional
114 transport direction of the parent flow. Embedded within the seismically chaotic, debrite-
115 dominated body of the MTCs, are packages of parallel, low-to-moderate amplitude reflections
116 that are often folded or faulted (e.g. Jackson 2011; Olafiranye *et al.* 2013; Alves 2015; Ortiz-
117 Karpf *et al.* 2017). We interpret these reflection packages as megaclasts that were
118 transported within the parent flow and preserved within the associated deposit (cf. Lee *et al.*
119 2004; McGilvery *et al.* 2004; Moscardelli *et al.* 2006; Dunlap *et al.* 2010). An alternative
120 interpretation is that these packages represent in-situ 'remnant blocks' (*sensu* Bull *et al.* 2009)
121 of substrate material, now flanked by debrite. However, their discordant bases and internal
122 deformation suggest they are not in-situ and have been transported.

123

124 *Offshore Colombia*

125 *Geological setting and data:* The Magdalena Fan is located along the Colombian-Caribbean
126 continental margin (Fig. 2) on the NE-trending South Caribbean Deformation Belt, in an area
127 of relatively subdued tectonic deformation between two main imbricate thrust belts. The
128 Magdalena Fan is fed by the Magdalena River and was deposited during a period of thin-
129 skinned compressional tectonic deformation; sediment input and stratigraphic architecture
130 are thus strongly structurally controlled (Romero-Otero 2009; Vinnels *et al.* 2010). We use a
131 Post-Stack Depth-Migrated 3D seismic survey to assess stacked Late Pleistocene MTCs that
132 coalesce above a composite basal surface (Ortiz-Karpf *et al.* 2016). Here, we focus on the
133 largest of these MTCs, referred to as C1 by Ortiz-Karpf *et al.* (2016, 2017; Fig. 3). Seismic
134 reflection data have a bin spacing of 12.5 x 12.5 m, a maximum frequency of 45 Hz, and a
135 dominant frequency of 30 Hz in the interval of interest; together, these parameters yield a
136 vertical resolution of c. 10-15 m and a horizontal resolution of c. 15 m.

137

138 *Description:* MTC C1 covers at least 400 km^2 and was likely sourced from, or near to, the shelf
139 edge (Ortiz-Karpf *et al.* 2016). The MTC was deposited on a structurally-deformed slope,
140 trending SE along the axis of a thrust-bound syncline, traversing a thrust-cored anticline
141 across a structural saddle, and extending to the W onto the largely undeformed basin floor
142 (Ortiz-Karpf *et al.* 2016). The basal surface of MTC C1 is erosive (200-500 m relief) and marked
143 by grooves that can be traced for up to 50 km, from the updip to the downdip limits of the
144 seismic dataset (Fig. 4). Above the thrust-cored anticlines, the lateral margins of the MTC are
145 steep and the basal surface is characterized by arcuate scarps that face inwards towards the
146 deposit. The top surface is irregular, tending to have most prominent relief (c. 150 m) directly
147 above contained megaclasts.

148

149 Internally, MTC C1 comprises debrite with megaclasts, which are 0.22-1.6 km long and 20-280
150 m thick, and are gently folded (Ortiz-Karpf *et al.* 2017). The majority of megaclasts have
151 rounded edges and are dispersed throughout the MTC, although there are concentrations
152 towards the lateral margins and to the W of the thrust-cored anticlines. Some megaclasts
153 occur in clusters overlying discrete erosional scours along the basal shear surface. Towards
154 the western limit of the dataset, the largest megaclasts overlie the eroded levee of an

underlying channel-levee complex where they are characterized by angular edges, and parallel internal reflections that are weakly to undeformed.

Interpretation: We infer that megaclasts in offshore Colombia formed: i) from direct degradation of the headwall scarp, based on the presence of grooves that can be traced to the updip limit of the dataset, towards the MTC source area (Ortiz-Karpf *et al.* 2017); ii) via local collapse of, or shearing from, the lateral margins, based on the development of arcuate scarps along the basal shear surface; and iii) from direct seabed entrainment, based on clustering of megaclasts above erosional scours developed along the basal shear surface.

Most of the megaclasts have rounded edges, suggesting some degree of abrasion against the basal shear surface or through direct impact with material carried within the debris-flow itself. Furthermore, most megaclasts are internally folded, suggesting they have been subjected to compressional and/or shear stress. Megaclast folding may have occurred during transport, or in-situ, prior to entrainment, due to compression of the substrate ahead of the confined flow (Jackson, 2011). The variety of megaclast sizes likely reflects their different origins, which may imply different compositions, degrees of consolidation, and/or transport distances. For example, the larger clasts may have been locally entrained or may have been mechanically more resistant, perhaps due to their lithification state; conversely, smaller clasts may be composed of weaker, possibly less lithified material, and/or were transported longer distances.

Offshore Brazil

Geological setting and data: The Santos Basin (Fig. 2) formed due to Cretaceous rifting and post-Cretaceous thermal subsidence. Late Cretaceous and Cenozoic erosion of the South American craton resulted in deposition of a thick clastic wedge along the NW basin margin (e.g. Modica & Brush 2004). This wedge is mudstone-rich and characterized by large (1.5–2.0 km high), SE-dipping clinoforms that are deformed by slope-perpendicular (i.e., NE-SW striking) normal faults (e.g. Modica & Brush 2004). This slope repeatedly failed during the Cretaceous and Cenozoic, with these events associated with deposition of MTCs on the slope and basin-floor (e.g. Modica & Brush 2004; Jackson 2011). We use a time-migrated, three-dimensional seismic reflection dataset to study a Cenozoic, megaclast-bearing MTC that was

187 derived from the upper slope and which covers ~3700 km^2 of the proximal basin-floor (Fig. 5).
188 The flow responsible for deposition of the MTC had a run-out distance of c.135 km and its
189 pathway partly controlled by partially confined, salt-controlled minibasins. In the interval of
190 interest, the seismic data have a vertical resolution of c. 10 m and a horizontal resolution of
191 12.5 m.
192
193 *Description:* Towards the NW, within a minibasin bounded by salt diapirs, the MTC is thickest
194 (up to 400 ms TWT) and contains megaclasts (0.3-10 km^2 in area, 200-380 ms thick) encased
195 in debrite . Most of the larger megaclasts are broadly rectangular in map view (Fig. 6) and
196 have sharp, sub-vertical contacts with the encasing debrite. The bases of the megaclasts sit
197 on, and locally define, the basal shear surface, which is sharp and incises up to 35 m into the
198 underlying units. Downdip of (i.e. to the SE) and lateral to (i.e. NE and SW) the minibasin the
199 MTC thins abruptly in all directions and eventually pinches out. Abrupt downdip thinning of
200 the MTCs suggests the salt diapirs were expressed at the seabed at the time of MTC
201 emplacement. Seismic-scale megaclasts are rare downdip of the minibasin, where the deposit
202 is inferred to be debrite-dominated. Locally, near the downdip terminus of the MTC, we
203 identify isolated packages of continuous, deformed, parallel reflections that resemble
204 substrate material, and which are embedded in the chaotic debrite (Fig. 6).
205
206 The basal shear surface of the MTC is characterized by broadly NE-trending striations that
207 developed within the minibasins and are absent 5 to 8 km beyond the minibasin edge (Fig. 6).
208 Striations trend SE, indicating the parent flow travelled from the NW, an interpretation
209 consistent with the overall geographical context (i.e. the coeval shelf edge lay to the NW) and
210 thickness of the MTC (i.e. the deposit pinches out towards the SE). In addition to the striations,
211 we also observe a series of larger-amplitude (10-60 ms TWT) up-stepping and down-stepping
212 ramps orientated broadly parallel (i.e. NW-trending) or perpendicular (i.e. NE-trending) to the
213 inferred parent flow direction (Figs 6, 7). Beneath the basal shear surface, the parallel
214 continuous reflections that constitute the substrate are locally deformed (Fig. 7).
215
216 Jackson (2011) indicate that the megaclasts are invariably deformed by two principle fold
217 types: (i) *frontal folds* – these anticlines characterize the megaclast frontal margins, and
218 directly overlie frontal ramps along the basal shear surface. Folds hinges, like the ramps they

219 overlie, trend perpendicular to the overall SE flow direction; and (ii) *lateral folds* – these
220 synclinal and anticlinal folds are developed at the lateral (i.e., NE and SW) margins of the
221 megaclasts and are typified by relatively steep (>10°) limb dips. Fold hinges are oriented
222 parallel to the SE flow direction. Additional anticlines, which are faulted and have relatively
223 steep (up to 25°) limb dips and hinges trending parallel to the rear of the megaclast (i.e.
224 perpendicular to the SE flow direction). Megaclasts are also internally folded, typically
225 adjacent to intra-megaclast faults, and contain moderately-to-steeply dipping (50°–75°)
226 normal faults that display maximum throws of 135 m. These faults are typically top truncated,
227 or rarely die out upward within the megaclasts. The strike of faults is highly variable both
228 within and between clasts, with common oblique to orthogonal intersections, and they do
229 not display a consistent geometric relationship to the overall SE transport direction of the
230 MTC. In addition to shear fractures (i.e. normal faults), opening mode fractures also occur
231 within megaclasts. These features display up to 500 m of horizontal extension, display variable
232 strikes, and are filled with inferred debritic material. These zones typically die out within or
233 may fully dissect, individual megaclasts.
234
235 *Interpretation:* In the Santos Basin, most large megaclasts were likely incorporated into the
236 MTC at its source and transported within the parent flow, rather than being eroded from the
237 seabed during passage of the parent flow. This interpretation is based on the following
238 observations: (i) the reflection character of the megaclasts matches that of material directly
239 landward of the headwall scarp; (ii) the height of the largest, best-preserved megaclasts
240 matches that of the headwall scarp; (iii) it seems unlikely that megaclasts, up to 350 m thick,
241 would be entrained from the seabed during passage of the parent flow, in which case we
242 might expect evidence of deeper erosion; and (iv) the long axis of large, rectangular
243 megaclasts invariably trend NE, which is consistent with them being derived from a
244 retrogressive failure process driving growth of the headwall scarp.
245
246 **Outcrop examples**
247 The studied deposits display many of the criteria typically used to identify MTCs. First, they
248 are dominated by poorly sorted muddy sandstone and sandy mudstone that define the
249 deposit matrix, and which support well-rounded extrabasinal clasts, or contorted intrabasinal
250 clasts. Second, they are bound by strata that follow the regional tectonic dip. Third, they are

bound at their bases by erosional surfaces or zones of distributed strain, which we interpret as basal shear surfaces or 'zones' (cf. 'kinematic boundary layer' of Butler *et al*. 2016). The contained megaclasts are identified by being: (i) supported by the poorly-sorted matrix; (ii) internally intensely deformed, with structures not following the more subtle, regional tectonic trends; and (iii) in some cases they are lithologically distinct to the surrounding stratigraphy.

Karoo Basin, South Africa

Geological setting: The Karoo Basin, South Africa has been interpreted as a retroarc foreland basin (Visser & Prackelt 1996), and more recently as a thermal sag basin that subsequently evolved into a retroarc foreland basin in the Triassic (Tankard *et al.* 2009). The infilling Karoo Supergroup is up to 8 km thick and is subdivided into the Dwyka, Ecca and Beaufort groups. An outcrop at Vriesgwaadg Farm [33°14'09"S, 21°52'36"E] exposes a 3 km long and 150 m high section of Permian clastic marine deposits of the Lower Ecca Group. The studied section is located at the distal end of the Laingsburg depocentre (Fig. 2). In this location, the Collingham Formation is overlain by the Vischkuil Formation, which comprises siltstone-rich turbidites and debrites that form the basal section of the 1800 m thick shallowing-upward succession from basin-floor deposits (Vischkuil and Laingsburg formations; van der Merwe *et al.* 2009), through channelized submarine slope (Fort Brown Formation; Hodgson *et al.* 2011), to shelf-edge and shelf deltas (Waterford Formation; Jones *et al.* 2015).

At Vriesgwaadg Farm, a section of Whitehill, Collingham and Vischkuil formations is overlain by several thick (10's m thick) MTCs, two of which are confined by 2-4.5 km wide and 60-90 m deep erosion surfaces, interpreted as basal shear surfaces (Fig. 8). Surface 1 incises older MTCs and the Collingham and Whitehill formations, whereas Surface 2 incises confined turbidites and younger MTCs. Overall, palaeoflow is towards the NE and E throughout the succession (Brooks *et al*. 2017).The mapping of successive slope-to-basin-floor systems in the Laingsburg depocentre indicates the presence of a broadly W-E trending, southern basin margin (van der Merwe *et al.* 2014), interpreted as the source slope of the MTCs (Brooks *et al*. 2017).

282 *Description:* Megaclasts are identified at several stratigraphic horizons, both overlying and
283 embedded within debrites, which contain m-scale, intraformational folded clasts (Fig. 8).
284 Megaclasts can be subdivided into two types. Type 1 clasts are 50-200 m long and 5-15 m
285 thick, comprise thin- to thick-bedded, sandstone-rich, normally graded turbidites. They are
286 sub-angular and elongate, and readily discernible from surrounding debrite, which is
287 sandstone- to siltstone-rich, and which contains mm-cm scale mudclasts throughout. Type 1
288 megaclasts are preserved within a topographic low formed by a concave basal shear surface.
289 The parent MTC partially infills this surface, and has a rugose top surface with minor (few
290 metres) relief onto which younger turbidites onlap. Type 2 clasts are 0.4-1 km long and 10-60
291 m high, consist of basin floor deposits of the underlying Whitehill and Collingham formations.
292 Layering within all clasts is subhorizontal, with the dip of coherent bedded sections generally
293 being weakly discordant (<10°) with the underlying and overlying turbidites. Type 2
294 megaclasts are sub-angular and elongate, with largely undeformed centres and primary
295 bedding structures, such as ripple laminations, preserved that indicate megaclasts were not
296 overturned. The margins of Type 2 megaclasts are faulted and highly disaggregated, with
297 sections of bedded strata (10's of centimetres to several metres in height and length) dipping
298 at high angles and locally being overturned. Type 2 megaclasts occur at the top of deformed
299 clast-rich, sandy MTCs, with clastic dykes, sourced from the sandy matrix, that fill fractures at
300 the megaclast peripheries. The MTC containing Type 2 megaclasts infills topographical lows
301 along the basal shear surface, with the megaclasts protruding above the top surface of the
302 deposit to form a highly rugose top surface onto which younger turbidite packages onlap.

303

304 *Interpretation:* Type 1 megaclasts are supported by their debritic, turbidite clast-bearing
305 matrix; we therefore interpret local entrainment and transport within the parent flow. The
306 entrainment of Type 2 megaclasts from substrate (the Whitehill and Collingham formations)
307 suggests the southern basin margin was tilted at the time of MTC emplacement (Brooks *et*
308 *al*. 2017). The weakly deformed interiors, angular shape and faulted nature of their margins
309 suggests Type 2 megaclasts were lithified prior to erosion and entrainment, and that their
310 margins were deformed as they collided with other debris during transport. Based on the
311 stratigraphic origin of these clasts, we interpret they were entrained from the substrate
312 during transport, rather than at the headwall of the parent flow. The location of Type 2

313 megaclasts at the top of MTCs indicates transport as rafted blocks, perhaps supported by
314 buoyancy or clast-to-clast interactions (e.g. Mulder & Alexander 2001; McGilvery *et al*.
315 2004). Alternatively, the megaclasts moved to the top of the flow, and were preserved
316 within the associated deposit through 'kinetic sieving' (Middleton & Hampton, 1976), or
317 moved as slide blocks over internal basal shear surfaces, remaining sub-parallel as they were
318 transported (Gee *et al.* 2006).

319

320 *Neuquén Basin, Argentina*

321 *Geological setting*: The Neuquén Basin covers 120,000km^2 and is located along the eastern
322 foothills of the Southern Central Andean cordillera, Argentina (Howell *et al.* 2005; Fig. 2). The
323 Neuquén Basin formed in response to Late Triassic to Early Jurassic rifting, Early Jurassic to
324 Early Cretaceous post-rift thermal subsidence, and Late Cretaceous to Cenozoic Andean
325 shortening (e.g. Vergani *et al*. 1995; Franzese & Spalletti 2001; Howell *et al*. 2005). At Chacay
326 Melehue, on Ruta 43 [37°16'01.00"S 70°31'43.00"W] is a well-exposed 7 km, E-W trending,
327 dip-orientated transect through the Middle Jurassic (Bathonian) Los Molles Formation. The
328 section comprises a laterally extensive, chaotic unit (10-60 m thick) that is underlain by a thick
329 claystone-prone interval with distinctive volcaniclastic beds that aid physical correlation, and
330 is overlain by a sandstone- (25 to 60 m thick) and then a mudstone-rich (450-500 m thick)
331 division (Fig. 9). The chaotic unit is a very poorly sorted, mud-rich sandstone matrix containing
332 granular quartz grains, rounded to well-rounded pebble and cobble clasts of metamorphic
333 and igneous origin, and abundant megaclasts (tens of metres in length), supporting a debrite
334 interpretation, . The basal shear surface is sharp and flat to slightly undulating. Locally, the
335 surface cuts steeply down into and then up through, the underlying substrate, which contains
336 multiple thrust faults and gravel dykes. Downdip, the basal shear surface thickens to form a
337 several metre-thick basal shear zone of high strain.

338

339 *Description:* Megaclasts (up to 200m long, 30 m thick) in the debrite comprise two lithologies
340 that occur in two distinct stratigraphic positions: (i) oyster-bearing conglomerate that is not
341 observed in the underlying stratigraphy, which is concentrated towards the base of the
342 chaotic unit, and have rounded edges; and (ii) thin-bedded, weakly deformed interbedded
343 turbiditic strata, which are concentrated towards the top of the chaotic unit and are relatively

undeformed and angular, containing open folds and low angle reverse faults. The conglomeratic megaclasts comprise well rounded igneous and metamorphic clasts.

Interpretation: The two megaclasts lithologies suggest entrainment occurred at two distinct times during MTC emplacement. Conglomeratic megaclasts with shallow-marine fauna were most likely derived from the headwall of the submarine landslide on the shelf, where broadly time-equivalent, compositionally similar, conglomerate-bearing successions occur (Veiga *et al.* 2013). In contrast, the thin-bedded turbiditic megaclasts were likely entrained as rafted blocks from the underlying substrate during emplacement. Their thin-bedded weakly deformed nature suggest the thin-bedded substrate was mostly lithified before entrainment. The occurrence of smaller (few metres diameter) clasts around the megaclasts suggest that either these have broken off from megaclasts during transport, or were entrained as smaller blocks from the local substrate. Commonly, thin-bedded megaclasts are located towards the top of the chaotic unit indicating granular convection supported by buoyancy, or were translated over internal shear surfaces and remained sub-parallel as they were transported (Gee *et al.* 2006).

Discussion

Mechanisms of megaclast entrainment

We here consider several mechanisms that may precondition the substrate, and ultimately result in entrainment of large fragments from the seabed during the passage of debris flows (Fig. 10).

Plucking: This process is similar to that occurring at the base of glaciers; i.e. entrainment of large pieces of bedrock driven by melting and freezing water under pressure in fractures (e.g. Rthlisberger & Iken 1981). In subaerial settings, entrainment of lithified substratum by mass movements occurs by plucking of fractured blocks of material from the bed (e.g. Stock & Dietrich 2006). In numerical models, Mitchell (2014) invokes plucking of large clasts as a key process responsible for material entrainment in bedrock-floored submarine canyons.

373

374 A similar process to plucking is envisaged beneath sediment gravity flows, involving the
375 detachment of substrate beneath highly energetic turbulent flows, either by shearing of scour
376 edges within a mobile, aggrading bed (e.g. Clark and Stanbrook 2001; Butler and Tavernelli
377 2006; Dykstra *et al.* 2011; Eggenhuisen *et al.* 2011), or by delamination or "hydraulic jacking"
378 (Puigdefàbregas *et al.* 2004; Eggenhuisen *et al.* 2011; Fonnesu *et al.* 2016; Fig. 10), a process
379 associated with injection of sand derived from the flow. Substrate disaggregation below
380 turbidity currents has been proposed to explain remobilization of metre-thick turbidite sand
381 (Butler & Tavarnelli 2006; Butler *et al.* 2016). This mechanism is associated with substrate
382 liquefaction by loading, enhanced by high-frequency reverberations caused by turbulence
383 within the overriding turbidity current (Røe & Hermansen 2006). A variant of entrainment via
384 plucking is 'enveloping'. The front of debris-flows are not always radial; instead, finger-like
385 projections are observed in some natural alluvial fan deposits (Hooke 1967; Suwa & Okuda
386 1983), and in physical experiments (Haas *et al.* 2016), giving the deposits an irregular edge. If
387 a frontally confined flow developed an uneven debris-flow front then large pieces of substrate
388 could be enveloped, and ingested as the flow propagated into the basin, or bevelled to form
389 remnant blocks (Fig. 1, 6).

390

391 *Deformation of substrate*: Deformation of the substrate is kinematically linked to the passage
392 of debris flow itself (Butler & McCaffrey 2010; Watt *et al.* 2012; Dakin *et al.* 2013), which can
393 precondition the substrate to entrainment of large fragments (Figs 10, 11). During deposit
394 emplacement, the body force from the confined debris flow is transmitted into the underlying
395 and adjacent substrate as a wave of compressional deformation (i.e. folding and thrusting),
396 with lateral shear being characterized by strike-slip-related deformation (Butler & McCaffrey
397 2011). Deformation can continue for as long as the shear stress induced by the flow exceeds
398 the critical shear stress of the substrate (Watt *et al.* 2012). Lateral loading of the substrate is
399 inferred from seismic examples (e.g. Moscardelli *et al.* 2006), being cited as a mechanism by
400 which the substrate is preconditioned to fail and thus permit entrainment of substrate
401 material in the form of megaclasts. Failure preconditioning by this mechanisms may be a
402 fundamental process governing the propagation and growth of the basal shear surface, such
403 as observed in bedding-plane controlled subaerial landslides (e.g. rupture propagation; Petley

404 *et al.* 2005; Watt *et al.* 2012). A similar process likely occurs in strata beyond the lateral
405 margins of a submarine debris flow (Alves 2015), with formation of a zone of distributed shear
406 ultimately leading to the development of imbricate thrusts (Watt *et al.* 2012). Substrate
407 deformation can also occur through shear coupling beneath an overriding flow. For example,
408 van der Merwe *et al.* (2009) demonstrate that high basal shear stresses coupled with a
409 vertical loading stress from an unconfined debris-flow triggered an underlying slide that was
410 developed above a much deeper décollement surface. Similar shear coupling processes have
411 been proposed in other large- and small-scale mass-transport deposits (Schnellmann *et al.*
412 2005; Minisini *et al.* 2007; Dasgupta 2008). Therefore, the basal shear might not, in fact, be a
413 discrete surface, but rather a zone, with the associated shear stresses distributed through a
414 thicker zone below the flow. A subsidiary process allowing megaclast entrainment is margin
415 failure; this may occur where the basal shear surface becomes underfilled during
416 emplacement (net degradation and bypass). In this case, the margin may fail by gravitational
417 collapse, with large fragments entrained into (i.e. if failure is syn-emplacement) or near the
418 top of (i.e. if post-emplacement) the flow (Bull *et al.* 2009).

419

420 *Evidence for megaclast entrainment processes from case studies:*
421 The arcuate scarps identified on the lateral margin of the basal shear surface offshore
422 Colombia (Fig. 4) are interpreted to record gravity-driven failure. In some cases, the arcuate
423 scarps are associated with normal faults that dip in towards the MTC, with these faults
424 accommodating failure of material and causing its eventual entrainment into the passing flow.
425 Sudden lateral unloading would likely result in a series of retrogressive failure events.

426

427 Ortiz-Karpf *et al.* (2017) interpret that dense packing of megaclasts towards the margins of
428 the MTCs (offshore Colombia) is a result of increased shear stress towards the base and lateral
429 margins of the parent flow, leading to entrainment from a progressively deepening basal
430 shear surface. Their interpretation is supported by the presence of clusters of megaclasts
431 above erosional scours, suggesting that, in some cases, the energy of the flow was insufficient
432 to transport the locally entrained material. In a similar way, the occurrence of large, relatively
433 undeformed megaclasts above the levee of an underlying channel-levee complex, indicates

local entrainment that could also be explained by locally elevated shear stresses as the levee was partially overridden by the debris flow (Ortiz-Karpf *et al.* 2017).

Although many of the large clasts were likely derived from the headwall source region, the presence of deformed seismic reflections in the substrate below the MTC offshore Brazil and partially disaggregated material towards its margins (Fig. 7), suggests the development of distributed shear zones. The ramps and flats developed along the basal shear surface (Fig. 6) may represent areas where substrate was entrained as megaclasts. Similar to the Colombia example, high shear stress at the base of the flow could have caused substrate deformation and subsequent erosion. Impingement of the cohesive flow against its margins could have deformed, weakened, and ultimately entrained the substrate (Fig. 10). Observations from our outcrop examples strengthen our hypothesis that substrate shear zone development is an important process in the entrainment of megaclasts. In the Neuquén Basin example, the basal shear *surface* thickens downstream into a *zone* (Fig. 9), suggesting the basal shear zone was progressively entrained in an upstream position. Enhanced preservation of the zone downstream suggests that shear rupture propagation might be an important consideration in development of basal shear surfaces in submarine landslide studies (Watt *et al.* 2012). Furthermore, the presence of a thick interval of thrusts, and the local presence of injectites sourced from the MTC (Fig. 9), suggests widespread substrate deformation may have helped entrain the megaclasts of turbiditic strata observed above the erosional base of the MTC.

Abrasion of megaclasts and impact on flow behaviour

The initial composition of a MTC, which is controlled by the protolith, can be markedly different to the final deposit as it rides over and entrains different substrate material (Piper *et al.* 1997; Lucennte & Pini 2003; Dykstra *et al.* 2011). Most of the material entrained from the substrate into an overriding mass flow will likely be poorly lithified (Mohrig *et al.* 1999). The resulting high pore-fluid pressure within the substrate lowers its bulk strength and leads to significant remobilization of the deposit (Dakin *et al.* 2013). Entrainment of different substrate types, for example the proportions of clay: silt: sand (Fig. 11), will impact the bulk grain-size distribution, and therefore temporal and spatial flow transformations, and the resulting deposit character (e.g., Iverson 1997; Dykstra *et al.* 2011; Joanne *et al.* 2013; Ortiz

Karpf *et al.* 2017). Similarly, during transport the megaclasts can be abraded or broken into smaller clasts (Fig. 11), which leads to changes in flow rheology and velocity.

Offshore Brazil, many internal structures are truncated at the megaclast margins, suggesting they formed early during the flow event and were progressively eroded at the clast margins during transport. The variable orientation of the intra-megaclast faults and folds with respect to the net-flow direction probably relates to complex, intraflow stress patterns that are not solely controlled by the overall flow motion towards the SE, but which at least partly reflect kinematic interaction of the megaclasts with the irregular basal shear surface. Offshore Colombia, the compositional variability of the substrate and complicated bathymetry is considered an important control on the behavior of subsequent flows, and the ultimate geometry of the associated MTCs (Ortiz Karpf *et al.* 2017)=. For example, the basal shear surface incised more deeply and eroded more substrate material from the sand-rich, poorly lithified material within channel-fills, compared to the more resistant, mud-prone, levees deposits.

Outcrop observations provide further evidence for the process of megaclast abrasion, and the importance in controlling the evolution of flow rheology. For example, in the Neuquén Basin example, the rounded edges of the shallow-marine conglomerate megaclasts, and the large high proportion of rounded clasts of similar igneous and metamorphic rock types in the debrite matrix to the conglomerate, suggest significant abrasion of these megaclasts during transport (Fig. 9). The degradation of megaclasts, whether entrained from the headwall, or during the bulking of the flow, will results in changes to the matrix strength and the flow character. The process and importance of megaclast abrasion and degradation has been identified in other locations. For example, Dykstra *et al.* (2011) discuss the effect of substrate entrainment on the compositional and rheological evolution of mass flows, documenting shearing of sand from entrained megaclasts into the matrix of an MTC at Cerro Bola, Argentina. They hypothesize that MTCs propagating over sandy substrates may become sandier downslope.

Conclusions

Here, we use case studies of megaclasts in debris flows from outcrop and subsurface data to illustrate their importance as key features of many MTCs, and highlight their potential role in changing flow behaviour. There is a complicated interrelationship between flow character, seabed topography, basal shear surface/zone development, entrainment of substrate as sediment and megaclasts, and abrasion and degradation of the megaclasts. We consider several mechanisms of entrainment, possible from a weakened substrate, which include i) plucking/delamination, ii) enveloping, and iii) distributed shear zones. The range of possible mechanisms for megaclast entrainment presented are not intended to be comprehensive or mutually exclusive. The development of an 'instantaneous' shear surface and a distributed shear zone, possibly developed through rupture propagation or shear coupling ahead of the flow front, is dynamic. As the zone propagates basinward the substrate will weaken and become preconditioned such that it is susceptible to entrainment as sediment and megaclasts. The entrainment, and subsequent abrasion, of the megaclasts will impact flow behaviour. The resulting flow transformations will be spatially and temporally complicated as the flow interacts with changes in seabed topography and variations in substrate with different degrees of compaction and lithification, and lithology. However, more work is needed to better constrain the relationships between the MTC, the basal shear zone, and the character and deformation of the substrate that might be linked to MTC emplacement in ancient deposits for outcrop and the subsurface. This can be complimented with physical and numerical modelling experiments. An integrated approach to the understanding of megaclast entrainment and abrasion will advance our predictive abilities to estimate the volumes and runout distances, and therefore the geohazard potential, of submarine landslides in modern continental margins.

520 REFERENCES

521 Alves, T. 2015. Submarine slide blocks and associated soft-sediment deformation in deep-
522 water basins: A review. *Marine and Petroleum Geology*, **67**, 262-285,
523 https://doi.org/10.1016/j.marpetgeo.2015.05.010.

524 Alves, T.M. & Cartwright, J.A. 2009. Volume balance of a submarine landslide in the Espírito
525 Santo Basin, offshore Brazil: quantifying seafloor erosion, sediment accumulation and
526 depletion. *Earth and Planetary Science Letters*, **288**, 572-580,
527 https://doi.org/10.1016/j.epsl.2009.10.020.

528 Alves, T.M. & Lourenço, S.D.N. 2010. Geomorphologic features related to gravitational
529 collapse: Submarine land sliding to lateral spreading on a Late Miocene–Quaternary slope (SE
530 Crete, eastern Mediterranean). *Geomorphology*, **123**, 13-33,
531 https://doi.org/10.1016/j.geomorph.2010.04.030.

532 Blair, T.C. & McPherson, J.G. 1999. Grain-size and textural classification of coarse sedimentary
533 particles. *Journal of Sedimentary Research*, **69**, 6-19.

534 Brooks, H.L., Hodgson, D.M., Brunt, R.L., Peakall, J. & Flint S.S. 2017. Exhumed lateral margins
535 and increasing confinement of a submarine landslide complex. *Sedimentology* (online).

536 Bull, S., Cartwright, J. & Huuse, M. 2009. A review of kinematic indicators from mass transport
537 complexes using 3D seismic data. *Marine and Petroleum Geology*, **26**, 1132–1151,
538 https://doi.org/10.1016/j.marpetgeo.2008.09.011.

539 Butler, R.W. & Tavarnelli, E. 2006. The structure and kinematics of substrate entrainment into
540 high-concentration sandy turbidites: a field example from the Gorgoglione 'flysch'of southern
541 Italy. *Sedimentology*, **53**, 655-670, https://doi.org/ 10.1111/j.1365-3091.2006.00789.x.

542 Butler, R.W.H. & McCaffrey, W.D. 2010. Structural evolution and sediment entrainment in
543 mass-transport complexes: outcrop studies from Italy. *Journal of the Geological Society,*
544 *London*, **167**, 617-631, https://doi.org/10.1144/0016-76492009-041.

545 Butler, R.W., Eggenhuisen, J.T., Haughton, P. & McCaffrey, W.D. 2016. Interpreting
546 syndepositional sediment remobilization and deformation beneath submarine gravity flows;
547 a kinematic boundary layer approach. *Journal of the Geological Society, London*, **173**, 46-58,
548 https://doi.org/10.1144/jgs2014-150.

549 Clark, J.D. & Stanbrook, D.A. 2001. Formation of large-scale shear structures during deposition
550 from high-density turbidity currents, Gres d'Annot Formation, south-east France. *In*:
551 McCaffrey, W.D., Kneller, B.C. & Peakall, J. (eds) *Particulate Gravity Currents*. International
552 Association of Sedimentologists Special Publication **31**, 219-232.

553 Dakin, N., Pickering, K.T., Mohrig, D. & Bayliss, N.J. 2013. Channel-like features created by
554 erosive submarine debris flows: Field evidence from the Middle Eocene Ainsa Basin, Spanish
555 Pyrenees. *Marine and Petroleum Geology*, **41**, 62-71.

Dasgupta, P. 2008. Experimental decipherment of the soft-sediment deformation observed in the upper part of the Talchir Formation (Lower Permian), Jharia Basin, India. *Sedimentary Geology*, **205**, 100-110.

Dunlap, D.B., Wood, L.J., Weisenberger, C. & Jabour, H. 2010. Seismic geomorphology of offshore Morocco's east margin, Safi Haute Mer area. *American Association of Petroleum Geologists Bulletin*, **94**, 615–642, https://doi.org/10.1016/j.marpetgeo.2008.09.011.

Dykstra, M., Garyfalou, K., Kertznus, V., Kneller, B., Milana, J.P., Molinaro, M., Szuman, M. & Thompson, P. 2011. Mass-transport deposits: Combining outcrop studies and seismic forward modelling to understand lithofacies distributions, deformation, and their seismic stratigraphic expression. *In*: Shipp, R.C, Weimer, P. & Posamentier, H. (eds) *Mass Transport Deposits in Deepwater Settings*. SEPM, Special Publication **96**, 293–310.

Eggenhuisen, J.T., McCaffrey, W.D., Haughton, P.D. & Butler, R.W. 2011. Shallow erosion beneath turbidity currents and its impact on the architectural development of turbidite sheet systems. *Sedimentology*, **58**, 936-959.

Festa, A., Ogata, K., Pini, G.A., Dilek, Y. & Alonso, J.L. 2016. Origin and significance of olistostromes in the evolution of orogenic belts: A global synthesis. *Gondwana Research*, **39**, 180-203.

Fonnesu, M., Patacci, M., Haughton, P.D., Felletti, F. & McCaffrey, W.D. 2016. Hybrid event beds generated by local substrate delamination on a confined-basin floor. *Journal of Sedimentary Research*, **86**, 929-943.

Franzese, J.R. & Spalletti, L.A. 2001. Late Triassic–early Jurassic continental extension in southwestern Gondwana: tectonic segmentation and pre-break-up rifting. *Journal of South American Earth Sciences,* **14**, 257–270, https://doi.org/10.1016/S0895-9811(01)00029-3.

Gamboa, D. & Alves, T.M. 2015. Three-dimensional fault meshes and multi-layer shear in mass-transport blocks: Implications for fluid flow on continental margins. *Tectonophysics*, **647-648**, 21-32, https://doi.org/10.1016/j.tecto.2015.02.007.

Gee, M.J.R., Gawthorpe, R.L. & Friedmann, S.J. 2006. Triggering and evolution of a Giant Submarine Landslide, Offshore Angola, revealed by 3D seismic stratigraphy and geomorphology. *Journal of Sedimentary Research*, **76**, 9-19, https://doi.org/ 10.2110/jsr.2006.02

Haas, T., Berg, W., Braat, L. & Kleinhans, M.G. 2016. Autogenic avulsion, channelization and backfilling dynamics of debris-flow fans. *Sedimentology*, **63**, 1596-1619.

Hampton, M.A., Lee, H.J. & Locat, J. 1996. Submarine landslides. *Reviews of Geophysics*, **34**, 33–59.

Hodgson, D.M., Di Celma, C.N., Brunt, R.L. & Flint, S.S. 2011. Submarine slope degradation, aggradation and the stratigraphic evolution of channel–levee systems. *Journal of the Geological Society, London*, **168**, 625–628. https://doi.org/10.1144/0016-76492010-177.

593 Hooke, R.L. 1967. Processes on arid-region alluvial fans. *The Journal of Geology*, **75**, 438-460.

594 Howell, J.A., Schwarz, E., Spalletti, L.A. & Veiga, G.D. 2005. The Neuquén Basin; an overview.
595 In: Veiga, G.D., Spalletti, L.A., Howell, J.A. & Schwarz, E. (eds) *The Neuquén Basin, Argentina;*
596 *a case study in sequence stratigraphy and basin dynamics*. Geological Society Special
597 Publications*,* **252**, 1-14.

598 Iverson, R. 1997. The physics of debris flows. *Reviews of Geophysics*, **35**, 245-296.

599 Jackson, C. A.-L. 2011. Three-dimensional seismic analysis of megaclast deformation within a
600 mass transport deposit; implications for debris flow kinematics. *Geology*, **39**, 203–206,
601 https://doi.org/10.1130/G31767.1.

602 Jackson, C. A.-L. & Johnson, H. 2009. Sustained turbidity currents and their interaction with
603 debrite-related topography; Labuan Island, offshore NW Borneo, Malaysia. *Sedimentary*
604 *Geology*, **219**, 77–96, doi:10.1016 /j.sedgeo.2009.04.008.

605 Joanne, C., Lamarche, C. & Collot, J.-Y. 2013. Dynamics of giant mass transport in deep
606 submarine environments: The Matakaoa Debris Flow, New Zealand. *Basin Research*, **25**, 471-
607 488.

608 Jones, G.E.D., Hodgson, D.M. & Flint, S.S. 2015. Lateral variability in clinoform trajectory,
609 process regime, and sediment dispersal patterns beyond the shelf-edge rollover in exhumed
610 basin margin-scale clinothems. *Basin Research*, **27**, 657-680.
611 https://doi.org/10.1111/bre.12092.

612 Kneller, B., Dykstra, M., Fairweather, L. & Milana, J.P. 2016. Mass-transport and slope
613 accommodation: Implications for turbidite sandstone reservoirs. *American Association of*
614 *Petroleum Geologists Bulletin*, **100**, 213-235.

615 Kvalstad, T.J., Andresen, L., Forsberg, C.F., Berg, K., Bryn, P. & Wangen, M. 2005. The Storegga
616 slide: evaluation of triggering sources and slide mechanics. *Marine and Petroleum Geology*,
617 **22**, 245–256.

618 Lee, C., Nott, J.A., Keller, F.B. & Parrish, A.R. 2004. Seismic expression of the Cenozoic mass
619 transport complexes, deepwater Tarfaya-Agadir Basin, offshore Morocco. Proceedings,
620 Offshore Technology Conference, Houston, Texas, article 16741,
621 https://doi.org/10.4043/16741-MS.

622 Lourenço, S.D., Sassa, K. & Fukuoka, H. 2006. Failure process and hydrologic response of a
623 two layer physical model: implications for rainfall-induced landslides. *Geomorphology*, **73**,
624 115-130.

625 Lucente, C.C. & Pini, G.A. 2003. Anatomy and emplacement mechanism of a large submarine
626 slide within a Miocene foredeep in the northern Apennines, Italy: A field perspective.
627 *American Journal of Science*, **303**, 565–602, https://doi.org/10.2475/ajs.303.7.565.

628 Marr, J.G., Harff, P.A., Shanmugam, G. & Parker, G. 2001. Experiments on subaqueous sandy
629 gravity flows: the role of clay and water content in flow dynamics and depositional structures.
630 *Geological Society of America Bulletin*, **113**, 1377–1386.

631 Martinsen, O.J. 1994. Mass movements. In: Maltman, A. (ed.) *The Geological Deformation of*
632 *Sediments*. Chapman & Hall, London, 127-165.

633 Masson, D.G., Van Niel, B. & Weaver, P.P.E. 1997. Flow processes and sediment deformation
634 in the Canary Debris Flow on the NW African Continental Rise. *Sedimentary Geology*, **110**,
635 163-179, https://doi.org/10.1016/S0037-0738(96)00089-9.

636 McGilvery, T.A., Haddad, G. & Cook, D.L. 2004. Sea floor and shallow subsurface examples of
637 mass transport complexes, offshore Brunei. Proceedings, Offshore Technology Conference,
638 Houston, Texas, article 16780.

639 Middleton, G.V. & Hampton, M.A. 1976. Subaqueous sediment transport and deposition by
640 sediment gravity flows. *In*: Stanley, D.J. & Swift, D.J.P (eds), *Marine Sediment Transport and*
641 *Environmental Management*, Wiley, New York, N.Y, 197-218

642 Minisini, D., Trincardi, F., Asioli, A., Canu, M. & Foglini, F. 2007. Morphologic variability of
643 exposed mass-transport deposits on the eastern slope of Gela Basin (Sicily channel). *Basin*
644 *Research*, **19**, 217-240.

645 Mitchell, N.C. 2014. Bedrock erosion by sedimentary flows in submarine canyons. *Geosphere*,
646 **10**, 892-904.

647 Modica, C. J. & Brush, E. R. 2004. Postrift sequence stratigraphy, paleogeography, and fill
648 history of the deep-water Santos Basin, offshore southeast Brazil. *American Association of*
649 *Petroleum Geologists Bulletin*, **88**, 923-945.

650 Mohrig, D., Elverhøi, A. & Parker, G. 1999. Experiments on the relative mobility of muddy
651 subaqueous and subaerial debris flows, and their capacity to remobilize antecedent deposits.
652 *Marine Geology*, **154**, 117-129, https://doi.org/10.1016/S0025-3227(98)00107-8.

653 Moscardelli, L., Wood, L. & Mann, P. 2006. Mass-transport complexes and associated
654 processes in the offshore area of Trinidad and Tobago. *American Association of Petroleum*
655 *Geologists Bulletin*, **90**, 1059–1088.

656 Mulder, T. & Alexander, A. 2001. The physical character of subaqueous sedimentary density
657 flows and their deposits. *Sedimentology*, **48**, 269–299, https://doi.org/10.1046/j.1365-
658 3091.2001.00360.x.

659 Olafiranye, K., Jackson, C.A.L. & Hodgson, D.M. 2013. The role of tectonics and mass-transport
660 complex emplacement on upper slope stratigraphic evolution: a 3D seismic case study from
661 offshore Angola. *Marine and Petroleum Geology*, **44**, 196-216.

662 Ortiz-Karpf, A., Hodgson, D.M. & McCaffrey, W.D. 2015. The role of mass-transport complexes
663 in controlling channel avulsion and the subsequent sediment dispersal patterns on an active

margin: The Magdalena Fan, offshore Colombia. *Marine and Petroleum Geology*, **64**, 58-75, https://doi.org/10.1016/j.marpetgeo.2015.01.005

Ortiz-Karpf, A., Hodgson, D.M., Jackson, C.A.-L. & McCaffrey, W.D. 2016. Mass-transport complexes as markers of deep-water fold-and-thrust belt evolution: Insights from the southern Magdalena Fan, offshore Colombia. *Basin Research*, https://doi.org/10.1111/bre.12208.

Ortiz-Karpf, A., Hodgson, D.M., Jackson, C.A-L. & McCaffrey, W.D. 2017. Influence of seabed morphology and substrate composition on mass-transport flow processes and pathways: insights from the Magdalena Fan, Offshore Colombia. *Journal of Sedimentary Research*, **87**, 189-209, https://doi.org/10.2110/jsr.2017.10.

Petley, D.N., Higuchi, T., Petley, D.J., Bulmer, M.H. & Carey, J. 2005. Development of progressive landslide failure in cohesive materials. *Geology*, **33**, 201-204.

Piper, D.J.W., Pirmez, C., Manley, P.L., Long, D., Flood, R.D., Normark, W.R. & Showers, W. 1997. Mass transport deposits of the Amazon Fan. *In*: Flood, R.D., Piper, D.J.W., Klaus, A., et al. (eds) Proceedings of the Ocean Drilling Program, Scientific Results, 155. Ocean Drilling Program, College Station, TX, 109–146.

Posamentier, H.W. & Kolla, V. 2003. Seismic geomorphology and stratigraphy of depositional elements in deep-water settings. *Journal of Sedimentary Research*, **73**, 367–388, https://doi.org/10.1306/111302730367.

Puigdefàbregas, C., Gjelberg, J. & Vaksdal, M. 2004. The Grès d'Annot in the Annot syncline: outer basin-margin onlap and associated soft-sediment deformation. In: Joseph, P. & Lomas, S. (eds) *Deep-Water Sedimentation in the Alpine Basin of SE France: New Perspectives on the Grès d'Annot and Related Systems*. Geological Society, London, Special Publications, **221**, 367-388.

Røe, S.L. & Hermansen, M. 2006. New aspects of deformed cross-strata in fluvial sandstones: examples from Neoproterozoic formations in northern Norway. *Sedimentary Geology*, **186**, 283-293.

Romero-Otero, G.A., 2009, *Deepwater sedimentary processes in an active margin, Magdalena submarine fan, offshore Colombia*. PhD Thesis, University of Oklahoma

Rthlisberger, H. & Iken, A. 1981. Plucking as an effect of water-pressure variations at the glacier bed. *Annals of Glaciology*, **2**, 57-62.

Sawyer, D.E., Flemings, P.B., Dugan, B. & Germaine, J.T. 2009. Retrogressive failures recorded in mass transport deposits in the Ursa Basin, Northern Gulf of Mexico. *Journal of Geophysical Research: Solid Earth*, **114 (B10)**.

Schnellmann, M., Anselmetti, F.S., Giardini, D. & McKenzie, J.A. 2005. Mass movement-induced fold-and-thrust belt structures in unconsolidated sediments in Lake Lucerne (Switzerland). *Sedimentology*, **52**, 271-289.

701 Sobiesiak, M.S., Kneller, B., Alsop, G.I. & Milana, J.P. 2016. Internal deformation and kinematic
702 indicators within a tripartite mass transport deposit, NW Argentina. *Sedimentary Geology*,
703 **344**, 364-381, https://doi.org/10.1016/j.sedgeo.2016.04.006.

704 Stock, J.D. & Dietrich, W.E. 2006. Erosion of steepland valleys by debris flows. *Geological*
705 *Society of America Bulletin*, **118**, 1125-1148.

706 Suwa, H. & Okuda, S. 1983. Deposition of debris flows on a fan surface, Mt. Yakedake, Japan.
707 *Zeitschrift für Geomorphology*, **46**, 79-101.

708 Tankard, A., Welsink, H., Aukes, P., Newton, R. & Stettler, E. 2009. Tectonic evolution of the
709 Cape and Karoo basins of South Africa. *Marine and Petroleum Geology*, **26**, 1379-1412,
710 https://doi.org/ 10.1016/j.marpetgeo.2009.01.022.

711 van der Merwe, W.C., Hodgson, D.M. & Flint, S.S. 2009. Widespread syn-sedimentary
712 deformation on a muddy deep-water basin-floor: the Vischkuil Formation (Permian), Karoo
713 Basin, South Africa. *Basin Research*, **21**, 389-406.

714 van der Merwe, W.C., Hodgson, D.M., Brunt, R.L. & Flint, S.S. 2014. Depositional architecture
715 of sand-attached and sand-detached channel-lobe transition zones on an exhumed stepped
716 slope mapped over a 2500 km^2 area. *Geosphere*, **10**, 1076-1093.

717 Veiga, G.D., Schwarz, E., Spalletti, L.A. & Massaferro, J.L., 2013. Anatomy and sequence
718 architecture of the early post-rift in the Neuquén Basin (Argentina): a response to
719 physiography and relative sea-level changes. *Journal of Sedimentary Research*, **83**, 746-765.

720 Vergani, G.D., Tankard, A.J., Belotti, H.J. & Welsink, H.J. 1995. Tectonic evolution and
721 paleogeography of the Neuquén Basin, Argentina. *In*: Tankard, A.J., Suarez Soruco, R. &
722 Welsink, H.J. (eds) *Petroleum Basins of South America*. *AAPG Memoirs*, 62, 383-402.

723 Vinnels, J. S., Butler, R. W. H., McCaffrey, W. D. & Paton, D. A. 2010. Depositional processes
724 across the Sinú accretionary prism, offshore Colombia. *Marine and Petroleum Geology*, **27**,
725 794–809, https://doi.org/10.1016/j.marpetgeo.2009.12.008.

726 Visser, J.N.J. & Prackelt, H.E. 1996. Subduction, mega-shear systems and Late Palaeozoic basin
727 development in the African segment of Gondwana. *Geologische Rundschau*, **85**, 632–646,
728 https://doi.org/10.1007/BF02440101.

729 Watt, S.F.L., Talling, P.J., Vardy, M.E., Masson, D.G., Henstock, T.J., Hühnerbach, V., Minshull,
730 T.A., Urlaub, M., Lebas, E., Le Friant, A. & Berndt, C. 2012. Widespread and progressive
731 seafloor-sediment failure following volcanic debris avalanche emplacement: Landslide
732 dynamics and timing offshore Montserrat, Lesser Antilles. *Marine Geology*, **323**, 69-94.
733

734 FIGURE CAPTIONS

735 **Fig. 1.** (**a**) Cartoon to illustrate the bulking up of submarine landslides down slope from
736 initiation failure, to entrainment of substrate during the passage of the flow. Matrix sediment
737 and megaclasts can be entrained at the headwall, and from the substrate, which could be
738 deformed prior to overriding by the flow. Adapted from Butler and McCaffrey (2010). (**b**) A
739 basal shear surface without the overlying deposit to illustrate features such as ramps and
740 flats, lineations, scours with megaclasts, and zones of deformation ahead of and to the side
741 of the deposit.

742 **Fig. 2.** Location maps for the four case studies of megaclasts in MTCs. (**a**) Location of 3D
743 seismic reflection survey from the Magdalena Fan, offshore Colombia. (**b**) Location of 3D
744 seismic reflection survey from the Santos Basin, offshore Brazil. (**c**) Location of the
745 Vriesgwaadg Farm outcrop, Laingsburg depocentre, Karoo Basin, South Africa. (**d**) Location of
746 the Chacay Melehue outcrop in the Neuquén Basin, Argentina.

747 **Fig. 3.** Perspective view of a variance extraction on the basal surface of the Magdalena Fan
748 MTC. The MTC was sourced from the shelf break and propagated above a structurally-
749 deformed slope, trending SE along the axis of a syncline, traversing an anticline across a
750 structural saddle, and continuing to the W onto the largely undeformed basin floor. On the
751 structurally-deformed slope, the basal surface is characterised by steep lateral margins.

752 **Fig. 4.** (**a**) Variance extraction on the basal surface of the MTC showing the distribution of the
753 megaclasts. Note the lineations on the basal surface, which are interpreted as grooves or
754 striations. (**b**) Seismic section across the downdip portion of the MTC showing megaclasts on
755 the lateral margins.

756 **Fig. 5.** (**a**) Perspective view of a variance extraction coloured by subsurface elevation of the
757 base surface of the MTC from the Santos Basin. Note the minibasins separated by salt highs.
758 (**b**) Seismic cross-sections along the MTC showing. Note the greater thickness of the MTC
759 within the largest minibasin and the presence of megaclasts.

760 **Fig. 6.** (**a**) Variance extraction on the basal surface of the MTC from the Santos Basin, showing
761 grooves or striations that occur mostly within the minibasins and disappear a few kilometres
762 downdip. The basal surface is characterised by up-stepping and down-stepping ramps with
763 variable orientations; the arrow indicated the down-thrown side of each ramp. (**b**) Variance

764 extraction across the middle of the MTC showing the downdip and areal variation in the
765 internal seismic character. Megaclasts are mostly present within the minibasins and the
766 deposit becomes more homogenous downdip.

767 **Fig. 7.** (**a**) Seismic cross-section towards the downdip margin of the MTC showing internally-
768 deformed, semi-continuous seismic reflections that resemble the surrounding substrate. (**b**)
769 Seismic cross-section across the minibasin showing internally-deformed, continuous
770 reflections towards the base of the MTC.

771 **Fig. 8.** (**a**) Panel of Vriesgewaagd Farm outcrop demonstrating the presences of megaclasts
772 both intercalated with and at the top of MTCs that infill large scale concave basal shear
773 surfaces (Surfaces 1 and 2). (**b**) Photopanel demonstrating the two types of megaclast
774 recognised at this outcrop, and the presence of clastic injectites through the fractured
775 margins of the megaclast. (**c**) Photopanel demonstrating the coherently bedded internal
776 sections of a megaclast and the disaggregated and faulted margins. The MTC and megaclast
777 create a rugose top surface onto which younger turbidite packages onlap.

778 **Fig. 9.** Location and geometries of megaclasts and basal shear surface in the MTC of Chacay
779 Melehue. (**a**) In the distal part of the outcrop, the basal shear 'zone' is preserved in the
780 underlying substrate. Angular megaclasts of thin-bedded turbiditic strata locally entrained
781 and located to the top of the MTC. Geologist as scale (1.85m). (**b**) Megaclasts of oyster-
782 bearing shallow-marine conglomerates are rounded and located at the base of the MTC near
783 a flat basal shear surface. (**c**) Large scale geometry of the MTC with megaclasts. Here the
784 deposit contains several locally entrained megaclasts, and the substrate is deformed by
785 multiple thrust faults and cross-cutting gravel injections. Bus for scale.

786 **Fig. 10.** Mechanisms of megaclast entrainment. (**a**) The emplacement of an erosionally
787 confined debris-flow can deform the substrate ahead, below, and to the sides of the flow,
788 such that it is weakened and liable to entrainment. (**b**) Megaclast could be entrained through
789 plucking or delamination of the substrate. (**c**) The weakened substrate could be enveloped
790 and entrained by a debris-flow with an uneven flow front. (**d**) If a distributed shear zone
791 developed ahead of the flow through shear rupture then thrust faults can be exploited.

792 Fig. 11. Cartoon to illustrate the interrelationships between flow character, seabed
793 topography, basal shear surface/zone, and the entrainment and abrasion of megaclasts. The

794 ‘instantaneous’ shear surface and the distributed shear zones are is dynamic, and propagate
795 basinward such that the substrate is weakened. The preconditioning of the substrate permits
796 entrainment as sediment and megaclasts. The entrainment, and subsequent abrasion of the
797 megaclasts will change the flow character, and therefore behaviour.
798

Figure 1

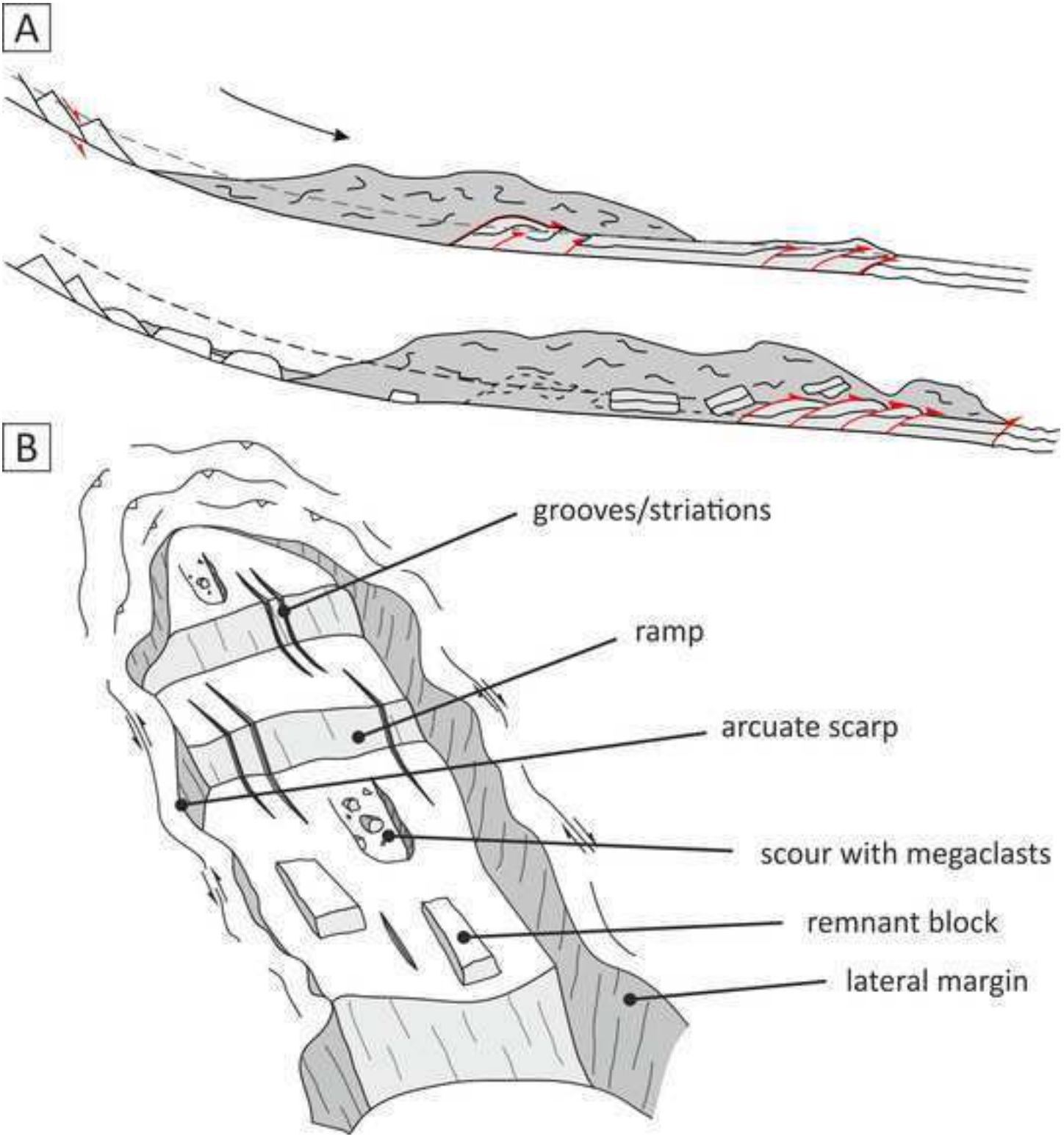
A
B
grooves/striations
ramp
arcuate scarp
scour with megaclasts
remnant block
lateral margin

Figure 2

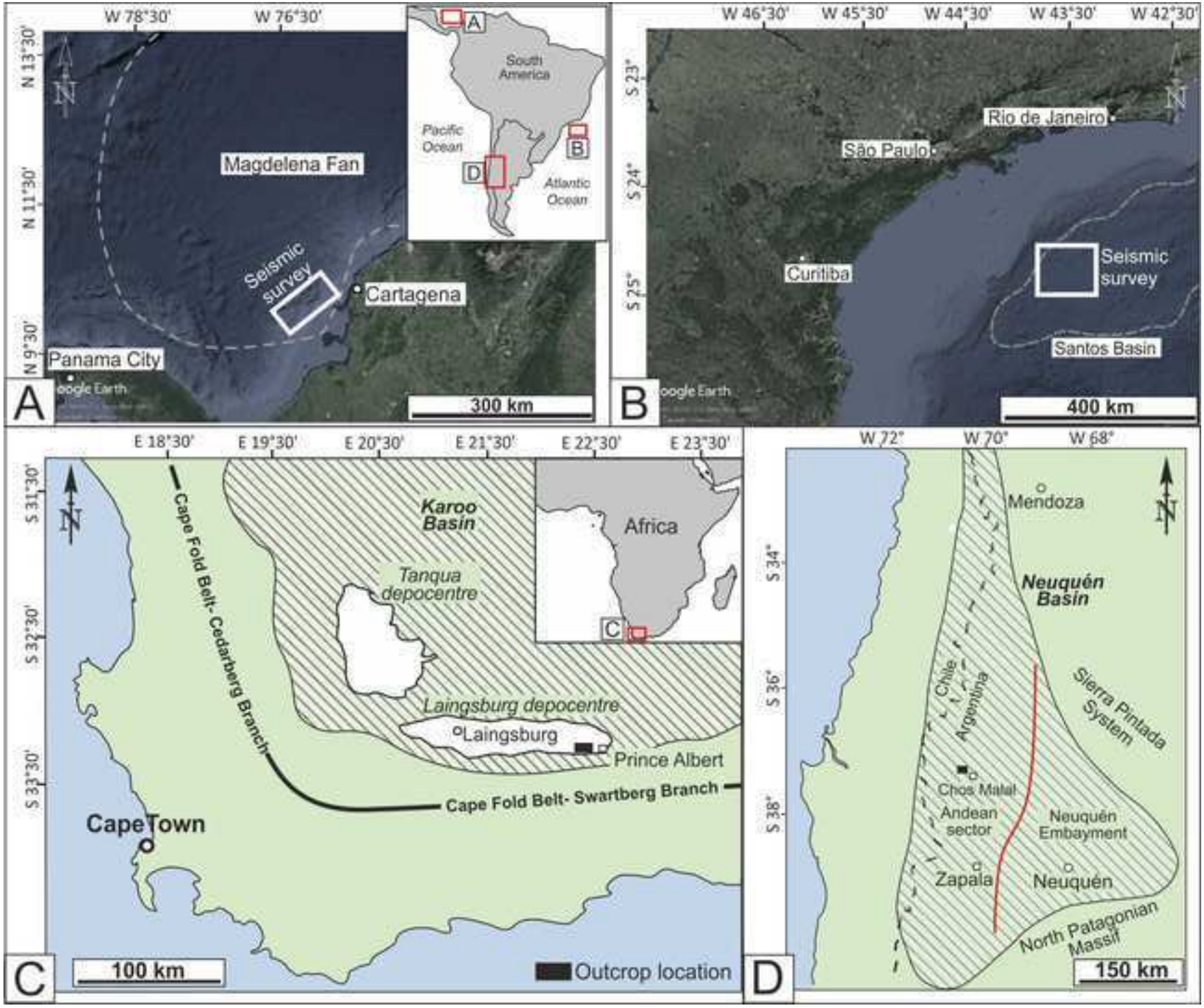
A
W 78°30'
W 76°30'
N 13°30'
N 11°30'
N 9°30'
Magdelena Fan
Seismic survey
Cartagena
Panama City
300 km
South America
Pacific Ocean
Atlantic Ocean
B
W 46°30'
W 45°30'
W 44°30'
W 43°30'
W 42°30'
S 23°
S 24°
S 25°
Rio de Janeiro
São Paulo
Curitiba
Seismic survey
Santos Basin
400 km
C
E 18°30'
E 19°30'
E 20°30'
E 21°30'
E 22°30'
E 23°30'
S 31°30'
S 32°30'
S 33°30'
Karoo Basin
Tanqua depocentre
Laingsburg depocentre
Laingsburg
Prince Albert
Cape Fold Belt- Cedarberg Branch
Cape Fold Belt- Swartberg Branch
CapeTown
Africa
100 km
Outcrop location
D
W 72°
W 70°
W 68°
S 34°
S 36°
S 38°
Mendoza
Neuquén Basin
Chile
Argentina
Sierra Pintada System
Chos Malal
Andean sector
Neuquén Embayment
Zapala
Neuquén
North Patagonian Massif
150 km

Figure 3

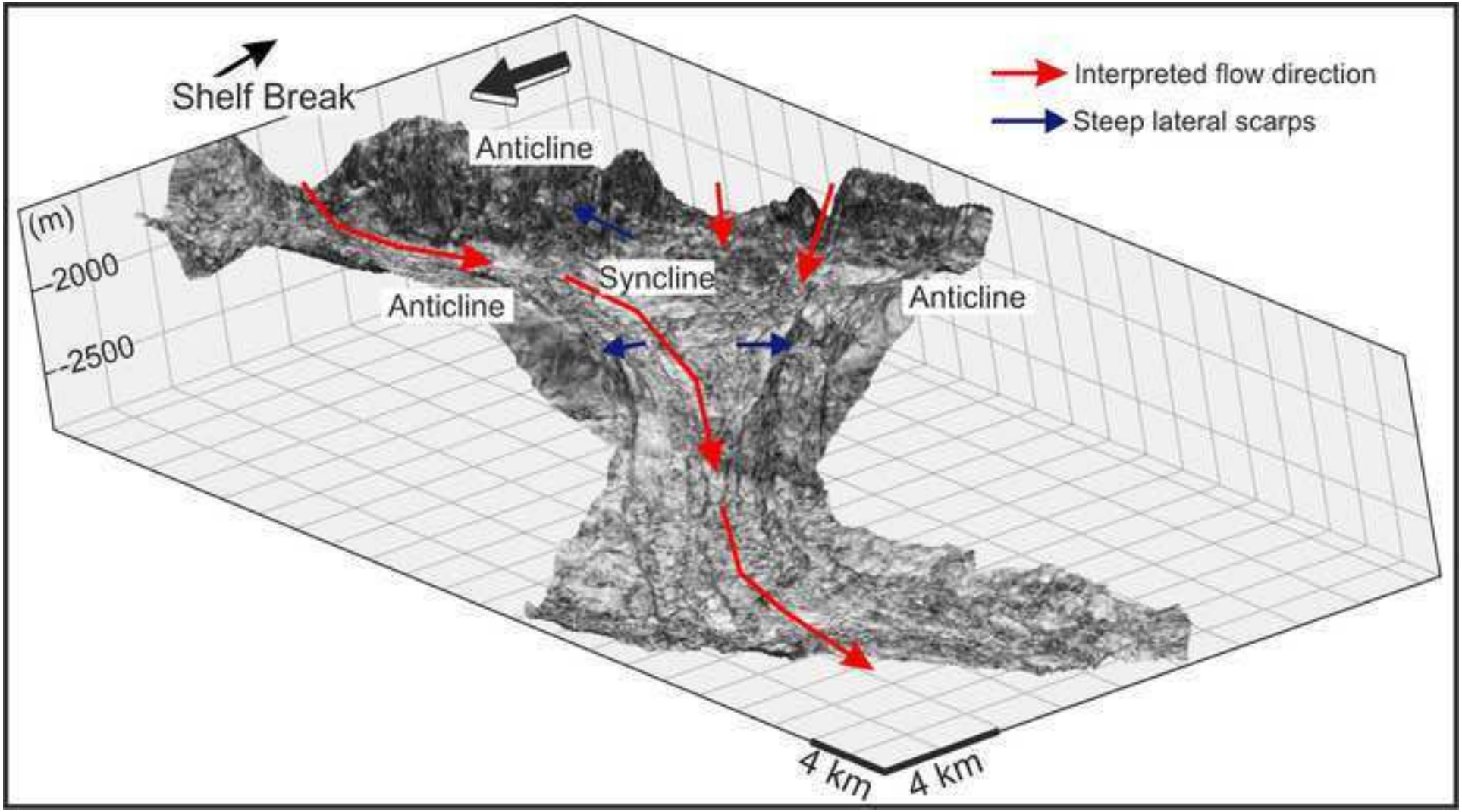
Shelf Break
Interpreted flow direction
Steep lateral scarps
Anticline
Anticline
Syncline
Anticline
(m)
-2000
-2500
4 km
4 km

Figure 4

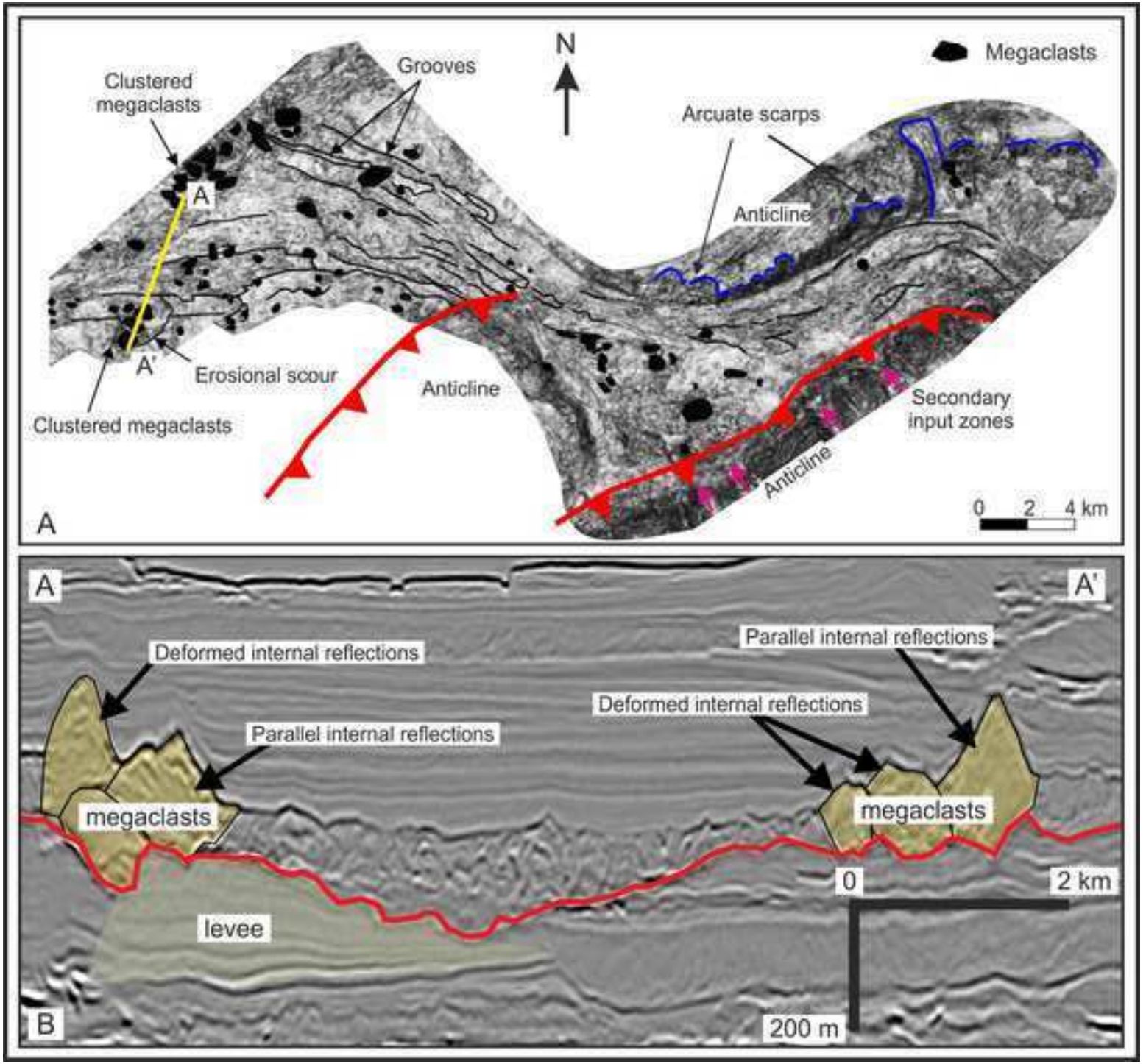
N
Megaclasts
Clustered megaclasts
Grooves
Arcuate scarps
Anticline
A
A'
Erosional scour
Anticline
Clustered megaclasts
Secondary input zones
Anticline
0 2 4 km
A
A
A'
Deformed internal reflections
Parallel internal reflections
Deformed internal reflections
Parallel internal reflections
megaclasts
megaclasts
0
2 km
levee
B
200 m

Figure 5

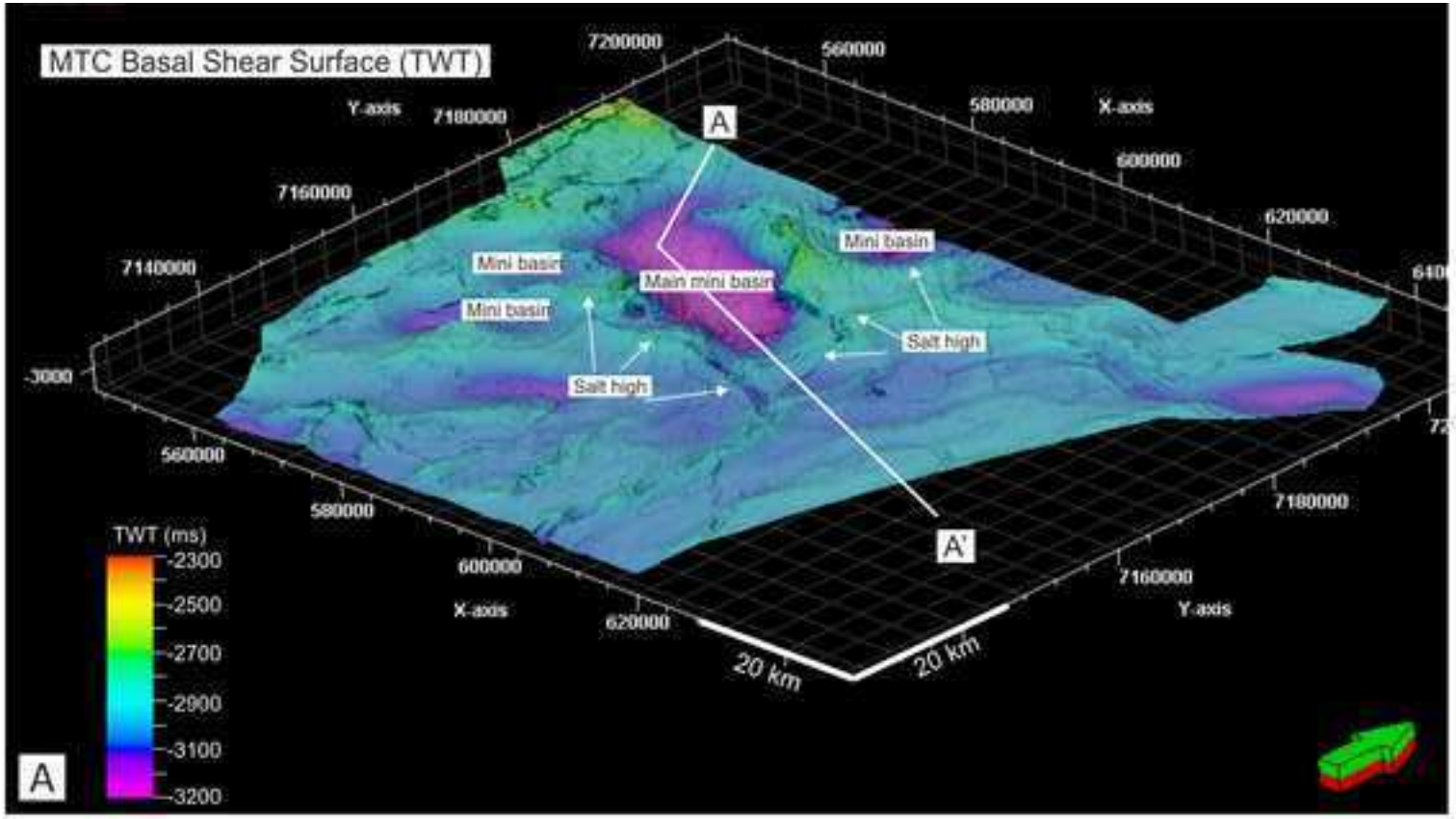
MTC Basal Shear Surface (TWT)
Y-axis
7200000
7180000
7160000
7140000
X-axis
560000
580000
600000
620000
A
A'
Mini basin
Main mini basin
Mini basin
Salt high
Salt high
TWT (ms)
-2300
-2500
-2700
-2900
-3100
-3200
20 km
20 km
A

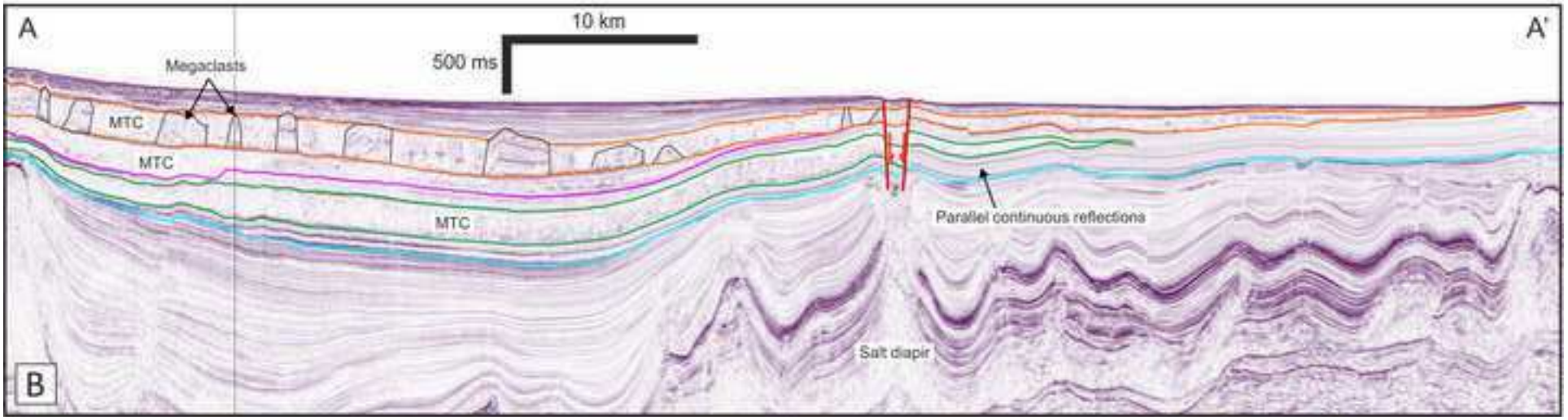
A
A'
10 km
500 ms
Megaclasts
MTC
MTC
MTC
Parallel continuous reflections
Salt diapir
B

Figure 6

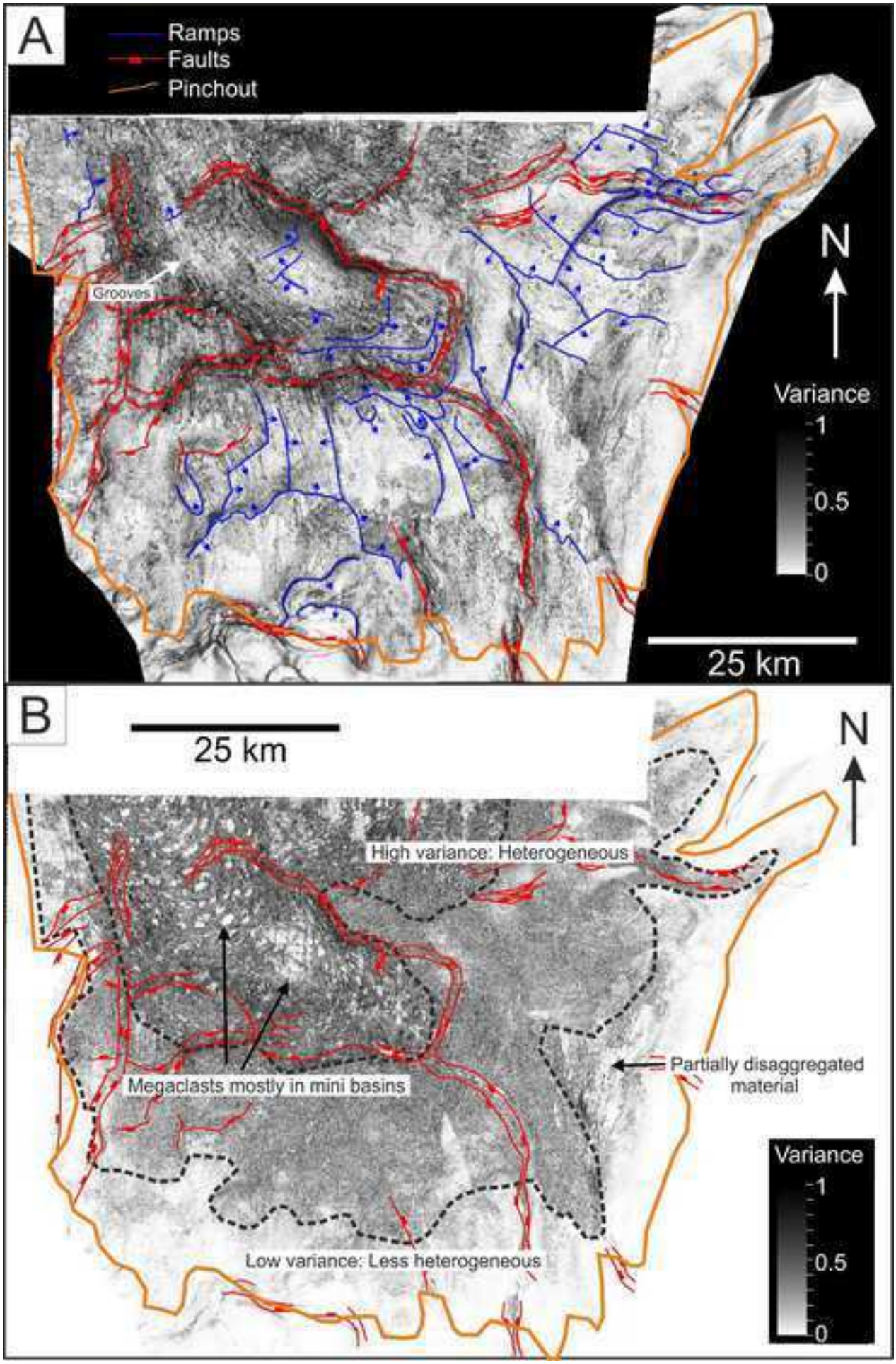
A
Ramps
Faults
Pinchout
Grooves
N
Variance
1
0.5
0
25 km
B
25 km
N
High variance: Heterogeneous
Megaclasts mostly in mini basins
Partially disaggregated material
Low variance: Less heterogeneous
Variance
1
0.5
0

Figure 7

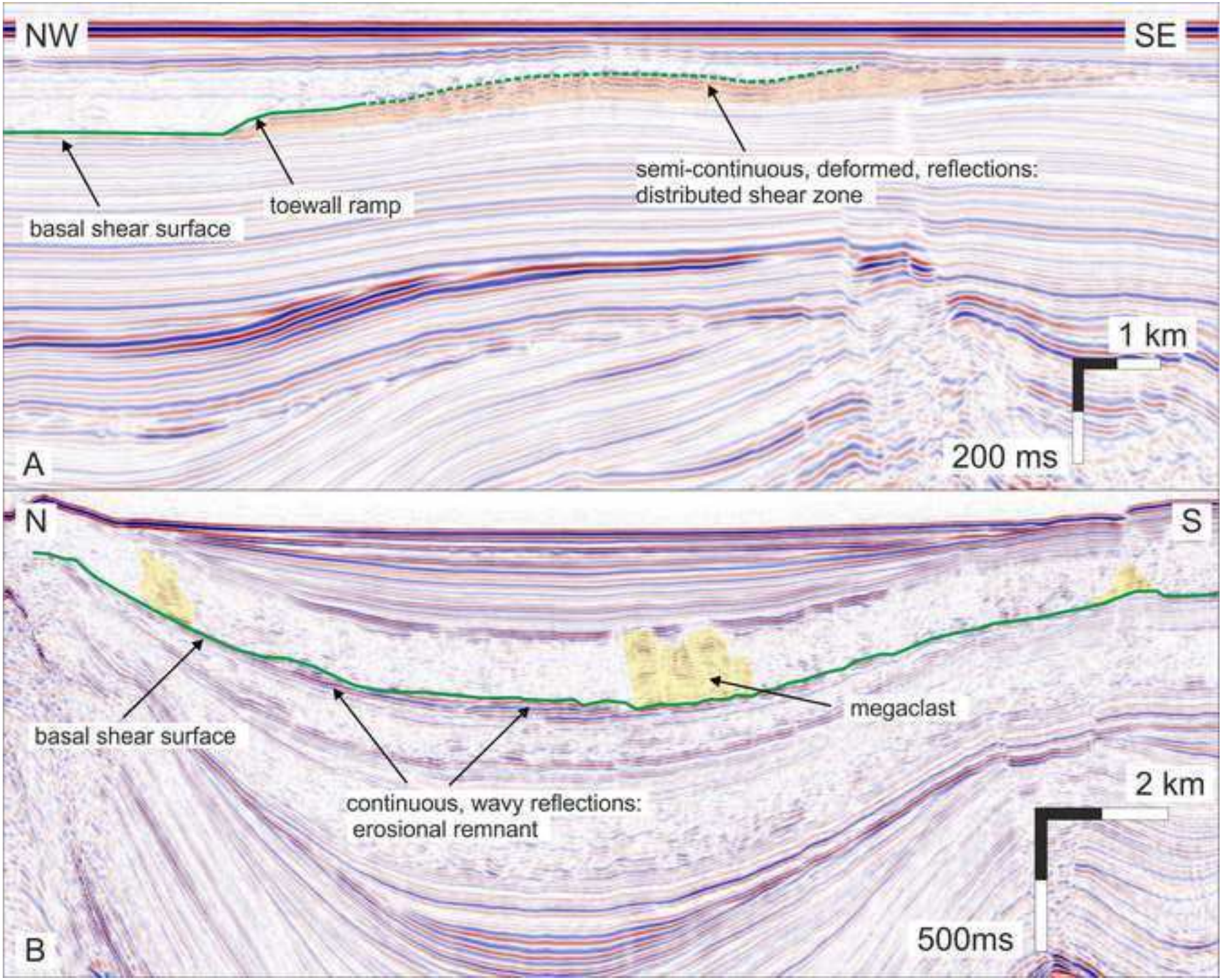
NW
SE
basal shear surface
toewall ramp
semi-continuous, deformed, reflections:
distributed shear zone
1 km
200 ms
A
N
S
basal shear surface
megaclast
continuous, wavy reflections:
erosional remnant
2 km
500ms
B

Figure 8

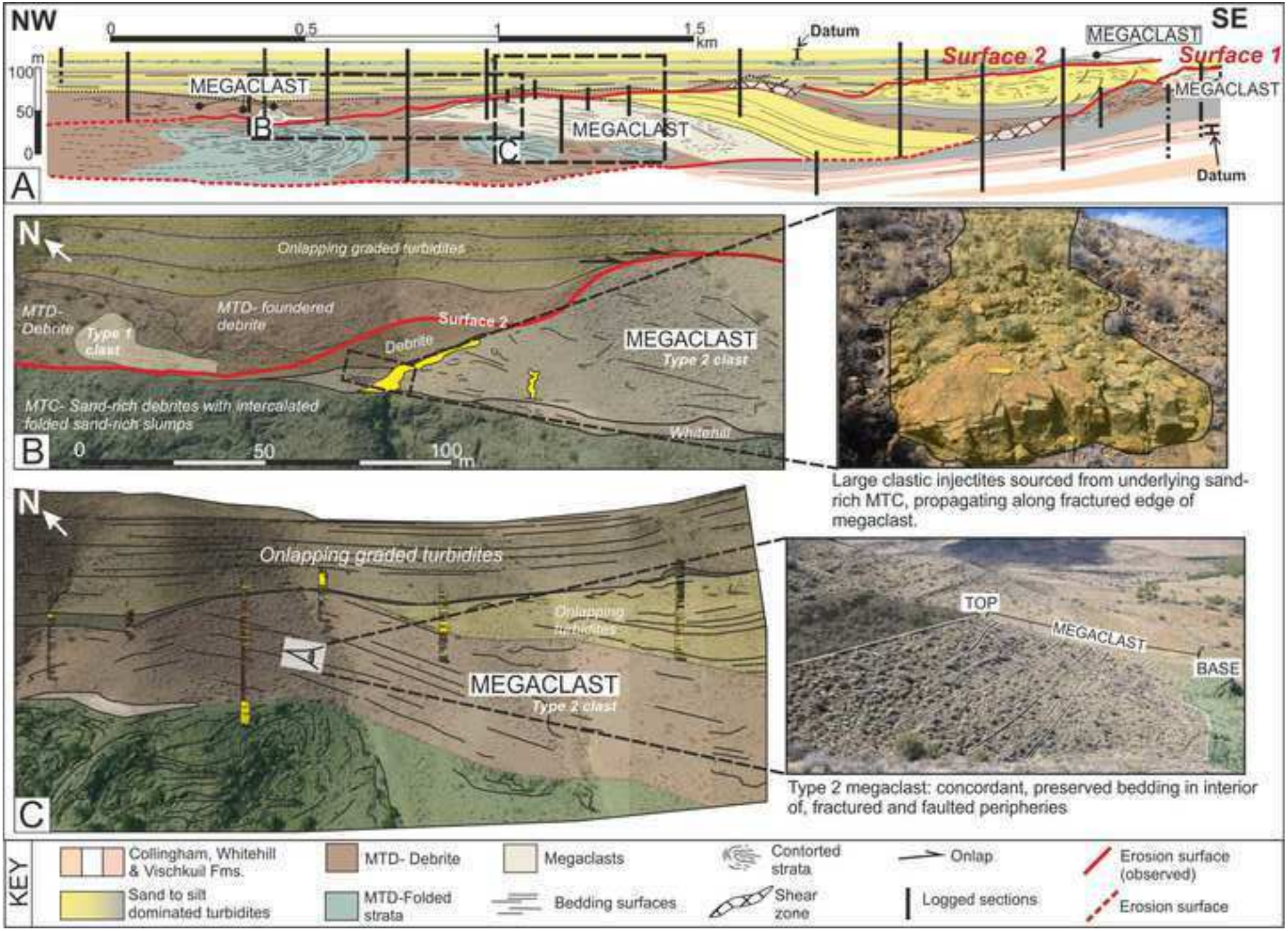
NW
SE
0
0.5
1
1.5
km
m
100
50
0
Datum
MEGACLAST
Surface 2
Surface 1
MEGACLAST
MEGACLAST
MEGACLAST
Datum
A
B
C
N
Onlapping graded turbidites
MTD-Debrite
Type 1 clast
MTD- foundered debrite
Surface 2
Debrite
MEGACLAST
Type 2 clast
MTC- Sand-rich debrites with intercalated folded sand-rich slumps
Whitehill
B
0
50
100 m
Large clastic injectites sourced from underlying sand-rich MTC, propagating along fractured edge of megaclast.
N
Onlapping graded turbidites
Onlapping turbidites
A
MEGACLAST
Type 2 clast
C
TOP
MEGACLAST
BASE
Type 2 megaclast: concordant, preserved bedding in interior of, fractured and faulted peripheries
KEY
Collingham, Whitehill & Vischkuil Fms.
Sand to silt dominated turbidites
MTD- Debrite
MTD-Folded strata
Megaclasts
Bedding surfaces
Contorted strata
Shear zone
Onlap
Logged sections
Erosion surface (observed)
Erosion surface

Figure 9

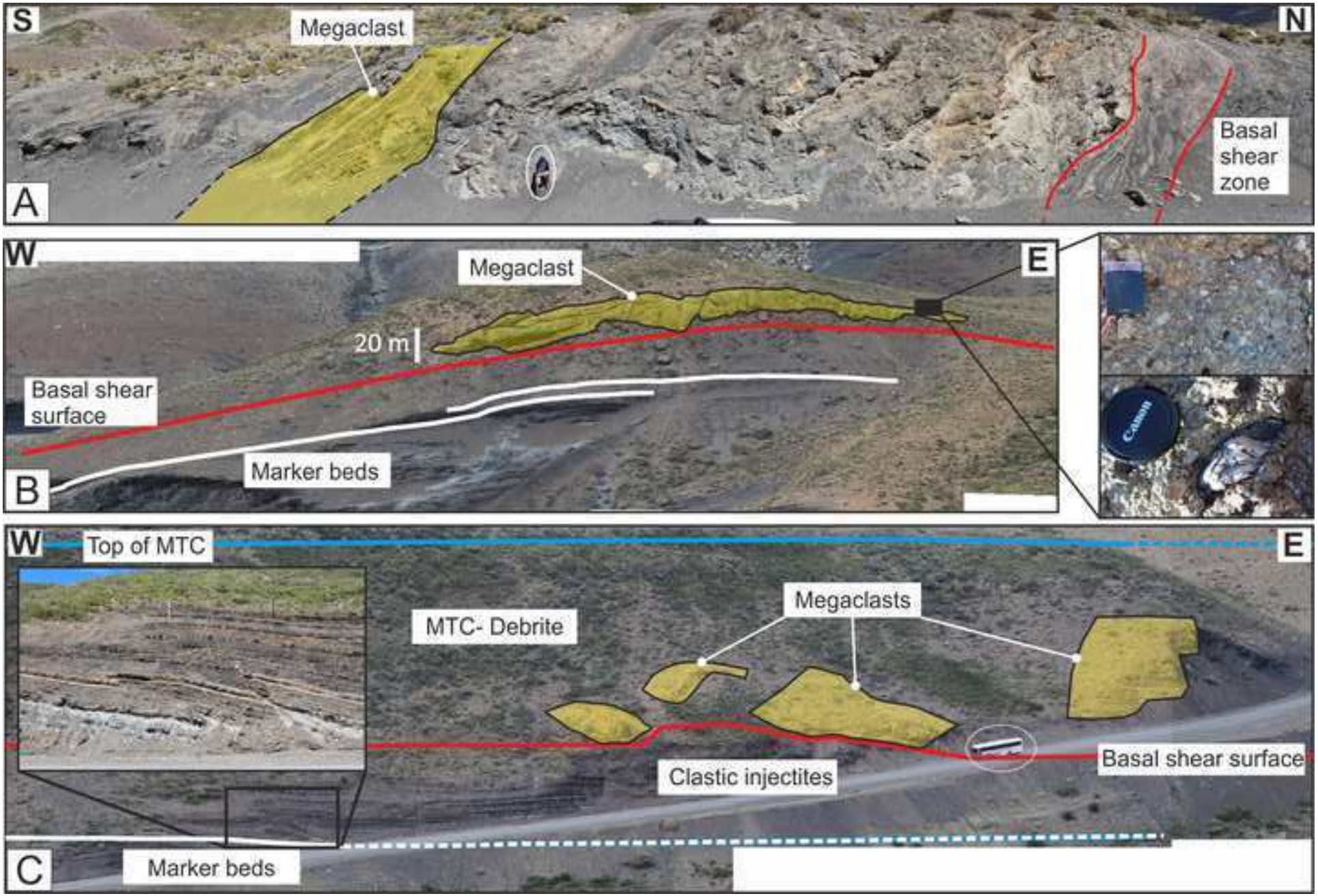
S
N
Megaclast
Basal shear zone
A
W
E
Megaclast
20 m
Basal shear surface
Marker beds
B
W
E
Top of MTC
MTC- Debrite
Megaclasts
Clastic injectites
Basal shear surface
Marker beds
C

Figure 10

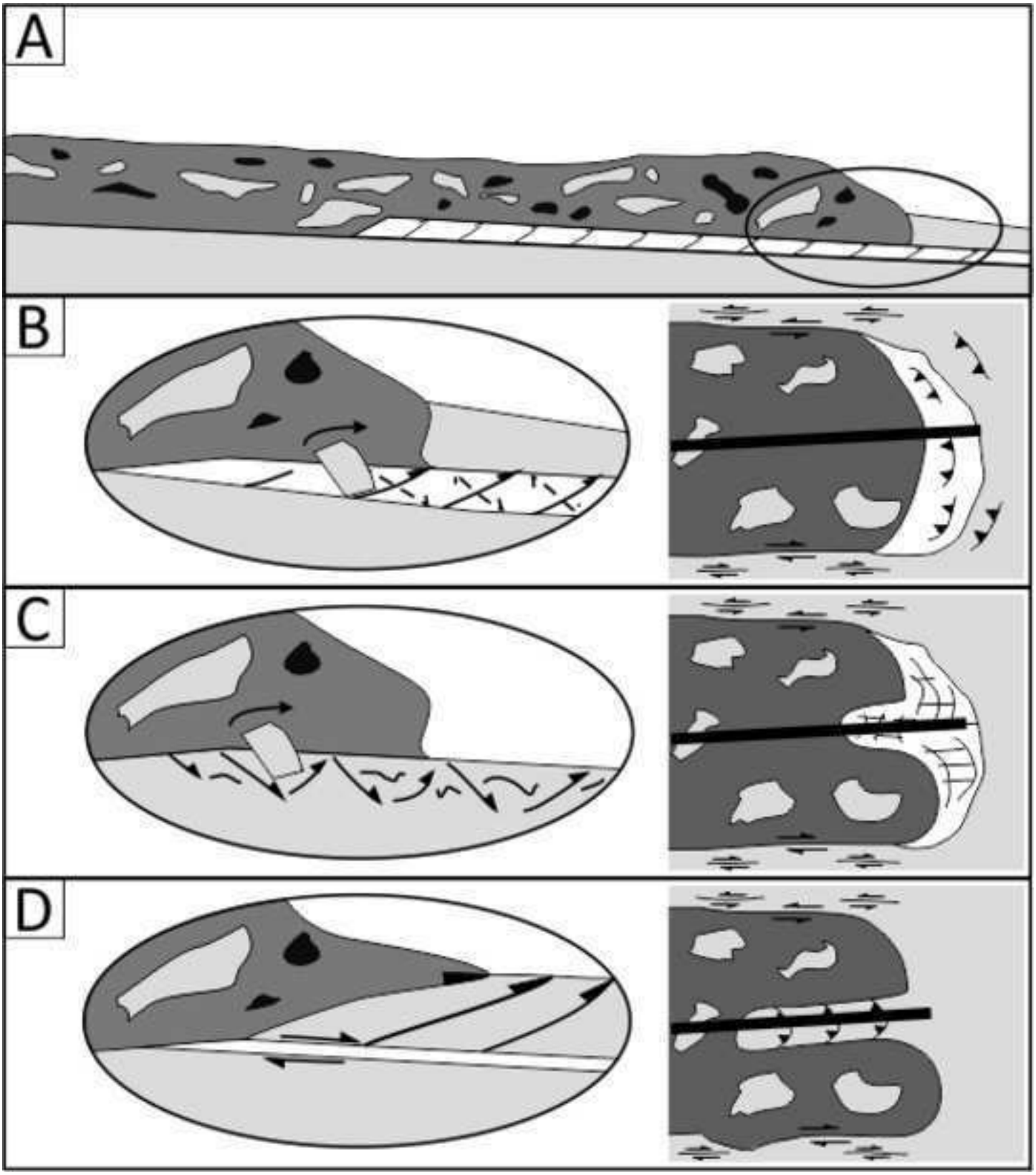

Figure 11

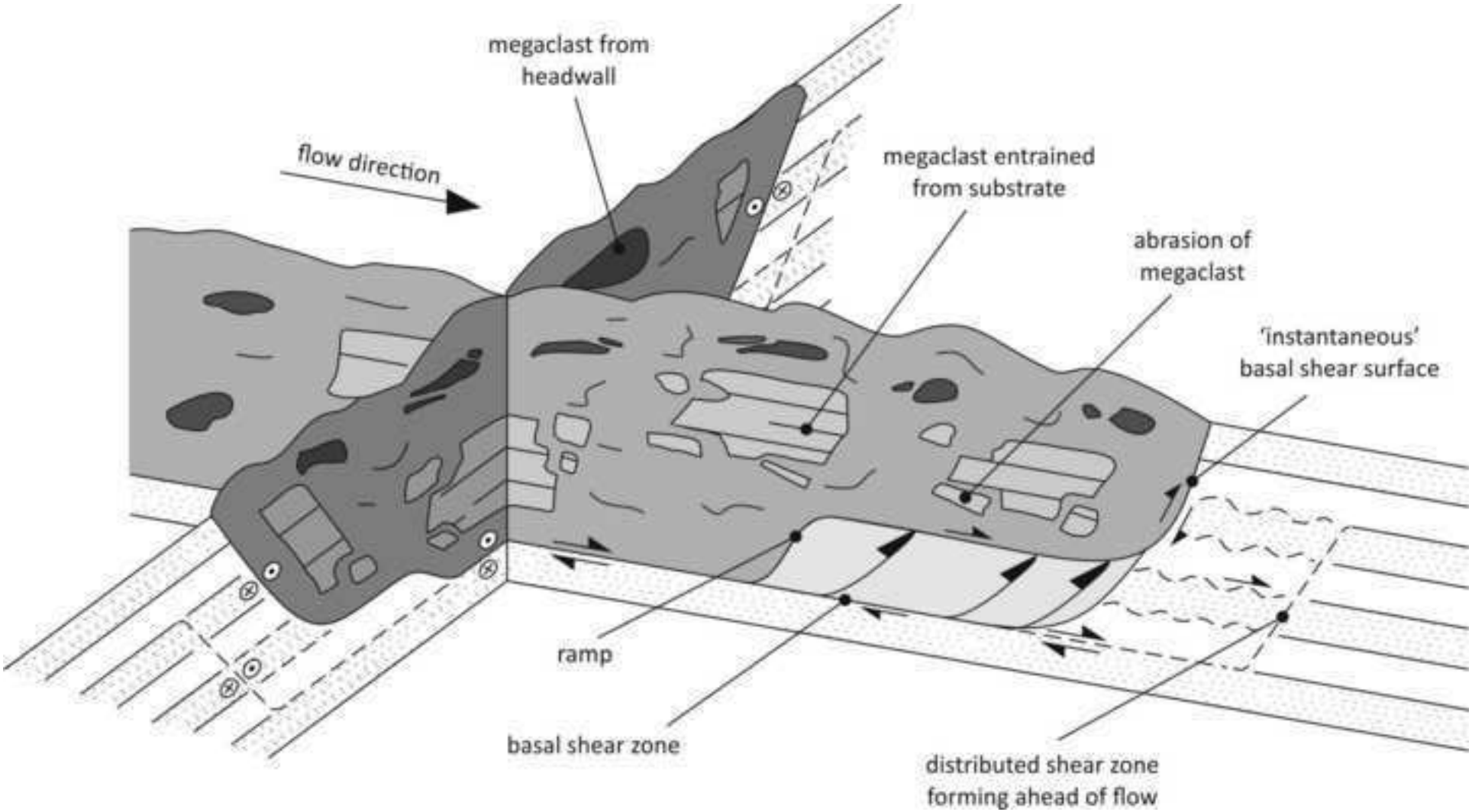
megaclast from
headwall
flow direction
megaclast entrained
from substrate
abrasion of
megaclast
'instantaneous'
basal shear surface
ramp
basal shear zone
distributed shear zone
forming ahead of flow